CENTRAL RESEARCH LIBRARY
DOCUMENT COLLECTION

ORNL-2012, Part IV
C-85 – Reactors-Aircraft Nuclear Propulsion Systems

AEC RESEARCH AND DEVELOPMENT REPORT

cy. 129A
ANP

DECLASSIFIED
Classification Changed To:
By Authority Of: AEC 1-25-56
By: G. Hasselmeier 2-14-67

MARTIN MARIETTA ENERGY SYSTEMS LIBRARIES
3 4456 0251027 2

AIRCRAFT NUCLEAR PROPULSION PROJECT

QUARTERLY PROGRESS REPORT

FOR PERIOD ENDING DECEMBER 10, 1955

CENTRAL RESEARCH LIBRARY
DOCUMENT COLLECTION
LIBRARY LOAN COPY
DO NOT TRANSFER TO ANOTHER PERSON
If you wish someone else to see this document, send in name with document and the library will arrange a loan.

OAK RIDGE NATIONAL LABORATORY
OPERATED BY
UNION CARBIDE NUCLEAR COMPANY
A Division of Union Carbide and Carbon Corporation
UCC
POST OFFICE BOX P • OAK RIDGE, TENNESSEE

RESTRICTED DATA
This document contains Restricted Data as defined in the Atomic Energy Act of 1954. Its transmittal or the disclosure of its contents in any manner to an unauthorized person is prohibited.

OAK RIDGE NATIONAL LABORATORY
OPERATED BY
UNION CARBIDE NUCLEAR COMPANY
UCC
POST OFFICE BOX X
OAK RIDGE, TENNESSEE

January 28, 1959

Central Research Library
4500

Report No.: ORNL-2012 Part IV Copy: 129A Classification: [redacted]

Author(s): W. H. Jordan, S. J. Cromer, A. J. Miller, A. W. Savolainen

Subject: Aircraft Nuclear Propulsion Project Quarterly Progress Report for Period Ending December 10, 1955.

Request compliance with indicated action:

Please make the following correction on your copy of the subject report.

The range of the ordinate of Fig. 14.4 on page 9 should be from 10^{-7} to 10^{-3} not from 10^{-8} to 10^{-4}.

N. T. Bray, Supervisor
Laboratory Records Department
Technical Information Division

NTB:WCB:dbt

ORNL:RC

[redacted]

ORNL-2012, Part IV
C-85 – Reactors-Aircraft Nuclear Propulsion Systems

This document consists of 42 pages.
Copy 129 of 205 copies. Series A.

Contract No. W-7405-eng-26

AIRCRAFT NUCLEAR PROPULSION PROJECT

QUARTERLY PROGRESS REPORT

For Period Ending December 10, 1955

W. H. Jordan, Director
S. J. Cromer, Co-Director
A. J. Miller, Assistant Director
A. W. Savolainen, Editor

DATE ISSUED

FEB 20 1956

OAK RIDGE NATIONAL LABORATORY
Operated by
UNION CARBIDE NUCLEAR COMPANY
A Division of Union Carbide and Carbon Corporation
Post Office Box P
Oak Ridge, Tennessee

[redacted]

MARTIN MARIETTA ENERGY SYSTEMS LIBRARIES

3 4456 0251027 2

[redacted]

INTERNAL DISTRIBUTION

1. R. G. Affel
2. C. R. Baldock
3. C. J. Barton
4. D. S. Billington
5. F. F. Blankenship
6. E. P. Blizard
7. C. J. Borkowski
8. G. E. Boyd
9. M. A. Bredig
10. F. R. Bruce
11. A. D. Callihan
12. D. W. Cardwell
13. J. V. Cathcart
14. C. E. Center (K-25)
15. R. A. Charpie
16. G. H. Clewett
17. C. E. Clifford
18. J. H. Coobs
19. W. B. Cottrell
20-21. D. D. Cowen
22. S. Cromer
23. R. S. Crouse
24. F. L. Culler
25. J. H. DeVan
26. D. A. Douglas
27. E. R. Dytko
28. L. B. Emlet (K-25)
29. M. J. Feldman
30. D. E. Ferguson
31. A. P. Fraas
32. J. H. Frye
33. W. T. Furgerson
34. H. C. Gray
35. W. R. Griffith
36. E. E. Hoffman
37. A. Hollaender
38. A. S. Householder
39. J. T. Howe
40. H. K. Jackson
41. W. H. Jordan
42. G. J. Keilholtz
43. C. P. Keim
44. M. T. Kelley
45. F. Kertesz
46. E. M. King
47-48. J. A. Lane
49. R. S. Livingston
50. R. N. Lyon
51. F. C. Maienschein
52. W. D. Manly
53. E. R. Mann
54. L. A. Mann
55. W. B. McDonald
56. F. R. McQuilkin
57. R. V. Meghreblian
58. R. P. Milford
59. A. J. Miller
60. R. E. Moore
61. K. Z. Morgan
62. E. J. Murphy
63. J. P. Murray (Y-12)
64. G. J. Nessle
65. R. B. Oliver
66. L. G. Overholser
67. P. Patriarca
68. R. W. Peelle
69. A. M. Perry
70. J. C. Pigg
71. W. G. Piper
72. H. F. Poppendiek
73. P. M. Reyling
74. H. W. Savage
75. A. W. Savolainen
76. R. D. Schultheiss
77. E. D. Shipley
78. A. Simon
79. O. Sisman
80. G. P. Smith
81. A. H. Snell
82. C. D. Susano
83. J. A. Swartout
84. E. H. Taylor
85. R. E. Thoma
86. D. B. Trauger
87. E. R. Van Artsdalen
88. F. C. VonderLage
89. G. M. Watson
90. A. M. Weinberg
91. J. C. White
92. G. D. Whitman
93. E. P. Wigner (consultant)
94. G. C. Williams

[redacted]

[redacted]

95. J. C. Wilson
96. C. E. Winters
97-106. ORNL-Y-12 Technical Library, Document Reference Section
107-126. Laboratory Records Department
127. Laboratory Records, ORNL R.C.
128-130. Central Research Library

EXTERNAL DISTRIBUTION

131. AF Plant Representative, Baltimore
132. AF Plant Representative, Burbank
133. AF Plant Representative, Marietta
134. AF Plant Representative, Santa Monica
135. AF Plant Representative, Seattle
136. AF Plant Representative, Wood-Ridge
137. Air Research and Development Command (RDGN)
138. Air Research and Development Command (RDZPA)
139. Air Technical Intelligence Center
140. Air University Library
141. Aircraft Laboratory Design Branch (WADC)
142-144. ANP Project Office, Fort Worth
145. Argonne National Laboratory
146. Armed Forces Special Weapons Project, Sandia
147. Assistant Secretary of the Air Force, R&D
148-153. Atomic Energy Commission, Washington
154. Bureau of Aeronautics
155. Bureau of Aeronautics General Representative
156. Chicago Operations Office
157. Chicago Patent Group
158-159. Chief of Naval Research
160. Convair-General Dynamics Corporation
161. Director of Laboratories (WCL)
162. Director of Requirements (AFDRD)
163. Director of Research and Development (AFDRD-ANP)
164-166. Directorate of Systems Management (RDZ-1SN)
167-169. Directorate of Systems Management (RDZ-1SS)
170. Equipment Laboratory (WADC)
171-174. General Electric Company (ANPD)
175. Hartford Area Office
176. Headquarters, Air Force Special Weapons Center
177. Lockland Area Office
178. Los Alamos Scientific Laboratory
179. Materials Laboratory Plans Office (WADC)
180. National Advisory Committee for Aeronautics, Cleveland
181. National Advisory Committee for Aeronautics, Washington
182. North American Aviation, Inc. (Aerophysics Division)
183. Nuclear Development Corporation
184. Patent Branch, Washington
185-187. Powerplant Laboratory (WADC)
188-191. Pratt & Whitney Aircraft Division (Fox Project)

[redacted]

[redacted]

192. Sandia Corporation
193. School of Aviation Medicine
194. USAF Project RAND
195. University of California Radiation Laboratory, Livermore
196-198. Wright Air Development Center (WCOSI-3)
199-204. Technical Information Extension, Oak Ridge
205. Division of Research and Development, AEC, ORO

[redacted]

[redacted]

FOREWORD

This portion, Part IV. Shielding Systems, of the Aircraft Nuclear Propulsion Project Quarterly Progress Report falls in AEC category C-85, Reactors – Aircraft Nuclear Propulsion Systems, and is therefore being issued separately in order not to further limit distribution of the material that falls in AEC category C-84, Reactors – Special Features of Aircraft Reactors, which has been issued as ORNL-2012, Parts I, II, III.

[redacted]

[redacted]

CONTENTS

FOREWORD v

SUMMARY 1

PART IV. SHIELDING SYSTEMS

14. TOWER SHIELDING FACILITY 5

GE R-1 Divided-Shield Mockup Experiments 5
Fast-Neutron Dose Rate Inside the Crew-Compartment Mockup 5
Radiation Measurements in the Crew Compartment as a Function of the Reactor Displacement from the *d* Axis 7
Fast-Neutron Dose-Rate Distribution in Air Around the Reactor Shield 8
Neutron Flux in Air as a Function of Distance from the Reactor Shield 10
TSF Reactor Power Determination 11

Calculation of the Contribution of Gamma Rays from Neutron Captures in Air to the Gamma-Ray Dose Rate Inside the G-E Crew-Shield Mockup 11
Determination of "Effective Thermal-Neutron Flux" 12
Calculation of Capture Gamma-Ray Dose Rate 13

Application of Differential Shielding Experiments to Predict Neutron Dose Rate in the GE R-1 Crew-Shield Mockup 16
Determination of Direct Radiation Around R-1 Mockup 16
Calculation of the Crew-Compartment Dose Rate 17
Calculation of Scattered Dose Rate in the Detector Tank 19

Procedure for the Optimization of a Unit Neutron Shield 19
Determination of Shield Weight 20
Calculation of Dose Rates 20
Application of Lagrange Multipliers 21

15. SHIELD WEIGHTS 25

Divided-Shield Weight Dependence on the Dimensions of a 300-Mw Circulating-Fuel Reactor 25
Gamma-Ray Shield 25
Neutron Shield 31
Total Shield Weights 31

[redacted]

[redacted]

ANP PROJECT QUARTERLY PROGRESS REPORT

SUMMARY

PART IV. SHIELDING SYSTEMS

14. Tower Shielding Facility

The experimental investigation of the shielding characteristics of the GE R-1 divided-shield mock-up has been concluded at the Tower Shielding Facility. The latest tests included measurements of the fast-neutron dose rates inside the crew shield both with a Hornyak button and with a Hurst-type dosimeter for a reactor-to-crew separation distance of 64 ft. Since some shielding groups have become interested in aircraft configurations in which the reactor and engines may be placed in the wings of the aircraft, the gamma-ray dose rate and neutron flux were also measured in the crew shield as a function of the horizontal displacement of the reactor from the crew-compartment axis. For displacements greater than 20 ft, rapid increases in the dose rates were observed. Measurements of the fast-neutron dose rate in air around the reactor shield were made in order to check the calculation of the fast-neutron leakage from the shield and to permit the calculation of the air-scattered neutron dose rate in the crew compartment. To distinguish between direct-beam and scattered neutrons, a neutron shadow cone (tank of borated water) was moved along the axis of the reactor and detector. Measurements off the front of the reactor shield showed that the direct beam contributed less than 25% of the total dose from fast neutrons. The neutron flux in air as a function of the distance from the reactor shield was measured for use in a calculation of the gamma-ray dose rate in the crew shield from neutron captures in air.

A discrepancy of a factor of 16 has been found between the measured gamma-ray dose rate in the G-E crew shield minus the calculated direct-beam dose rate and the calculated dose rate from scattered gamma rays. In an investigation to determine whether this discrepancy can be attributed to neutron captures in air, the air capture gamma-ray dose rate in the crew shield was calculated to be approximately 4×10^{-7} mr/hr·watt. Since the calculated direct-beam dose rate (6.6×10^{-8} mr/hr·watt) and the calculated air-scattered dose rate (3.9×10^{-8} mr/hr·watt) only totaled 1.05×10^{-7} mr/hr·watt and the total measured dose rate was 7×10^{-7} mr/hr·watt, it does appear that neutrons captured by air contribute significantly to the total gamma-ray dose rate.

The method of calculation in which scattering probabilities previously determined from the differential shielding experiments were used was applied to predict the fast-neutron dose rate in the GE R-1 crew compartment. The calculated dose rate then was compared with the measured dose rate. The total dose rate was calculated to be 8×10^{-8} mrep/hr·watt. The measured dose rate was 2.5×10^{-8} mrep/hr·watt, a factor of 3.2 lower than the calculation would indicate. The calculation did not take into account the ducts in the reactor shield, which would give rise to radiation that would have, in penetrating the crew compartment, relaxation lengths shorter than those used in the calculation. In order to investigate this further, a calculation of the scattered fast-neutron dose rate in the TSF detector tank as a function of effective water thickness was carried out. A comparison of the results with experimental measurements indicated that the relaxation lengths used in the calculation were too high by a factor of 1.3 to 2.3. However, extrapolation of the calculated and measured curves indicated agreement at the surface.

A procedure for optimizing a unit neutron shield by using TSF experimental data has been developed. As was outlined in the optimization procedure for the divided shield, the reactor shield assembly is divided into N conical shells. The total weight and the total dose rate (scattered and direct) at a given distance from the reactor shield are both expressed as functions of the shield thickness. The shield weight is minimized by utilizing the method of Lagrange multipliers. The method was used to calculate the weight for a 90-Mw reactor and an assumed $\cos^{10}\theta$ distribution of neutrons at the shield surface. For a 5.9-mrem/hr neutron dose rate at a distance of 41 ft, the total water shield weight was calculated to be 39,900 lb. For 24 mrem/hr, the weight was 30,200 lb.

[redacted]

15. Shield Weights

The parametric divided-shield weight study for 300-Mw, circulating-fuel, reflector-moderated reactors was completed. Total weights of the reactor, reactor shield, and crew-compartment shield were calculated for various power densities, island radii, heat exchanger thicknesses, and reflector thicknesses. The calculations were based on data from LTSF circulating-fuel reflector-moderated reactor experiments, data from TSF differential shielding experiments, a divided-neutron-shield optimization procedure, and the NDA single-scattering penetration probabilities for gamma rays. For a total dose rate inside the crew compartment of 1 rem/hr, the total reactor and shield weights varied between 56,000 and 99,000 lb for power densities of 1.375, 2.750, 4.125, and 5.500 kw/cm^3; island radii of 0, 4, and 8 in.; beryllium reflector thicknesses of 8, 10, 12, and 16 in.; and heat exchanger thicknesses of 3.5, 6.5, and 8.0 in.

Part IV

SHIELDING SYSTEMS

14. TOWER SHIELDING FACILITY

C. E. Clifford
J. L. Hull F. L. Keller
F. J. Muckenthaler F. N. Watson
Applied Nuclear Physics Division
G. J. Rausa
The Martin Company

Experiments with the GE R-1 divided-shield mockup have been completed. In an attempt to explain the high measured gamma-ray dose rate in the crew compartment, the contribution to the gamma-ray dose by neutrons captured in air was investigated. The measured neutron dose in the crew compartment was compared with a calculated value. The calculation utilized modified scattering probabilities derived from data obtained during the differential experiments and fast-neutron dose measurements in air around the R-1 reactor shield.

A procedure for the optimization of a unit neutron shield has been developed that makes use of Tower Shielding Facility (TSF) data.

GE R-1 DIVIDED-SHIELD MOCKUP EXPERIMENTS

F. N. Watson

The concluding experiments on the shielding characteristics of the GE R-1 reactor shield (Fig. 14.1) and the crew-compartment shield (Fig. 14.2) included: (1) measurements of the fast-neutron dose rates in the crew compartment; (2) measurements of gamma-ray and fast-neutron dose rates in the crew compartment as a function of the horizontal displacement of the reactor from the crew-compartment (or fuselage) axis; (3) measurements of the fast-neutron dose rates in the air around the reactor shield, with and without a shadow shield, in an effort to determine the magnitude of the direct-beam-neutron dose rate; and (4) measurements of the thermal-neutron flux outside the reactor shield. Gamma-ray dose-rate measurements taken in the air outside the reactor shield, with and without a shadow shield, will be reported at a later date.

The description of the geometry of the TSF experiments has been presented in several previous reports and will not be repeated here. However, the following definitions should be remembered:

d axis = horizontal axis of reactor and crew compartment in their normal positions,

h = height of d axis from ground,

x = distance along a horizontal axis of the crew compartment, perpendicular to the d axis,

y = distance along the horizontal axis of the crew compartment that coincides with the d axis,

z = distance along vertical axis of the crew compartment,

x_0, y_0, z_0 = point on d axis at rear face of the crew compartment,

θ = angle of radiation emission measured with respect to the d axis.[1]

Fast-Neutron Dose Rate Inside the Crew-Compartment Mockup

The fast-neutron dose rates at various points inside the crew-compartment mockup of the R-1 shield were measured. Because the Hurst-type dosimeter usually used for fast-neutron measurements at the TSF has low sensitivity, a 5-in.-dia Hornyak-button scintillation counter[2] that is three times more sensitive than the dosimeter was used. [Exposure of a nine-chamber dosimeter produces only about 40 counts/min for the approximately 0.008-mrep/hr dose rate in the crew compartment (reactor power = 400 kw).]

The measurement of the dose rate near the center of the crew compartment was made both with the Hornyak button and with the Hurst-type dosimeter. The agreement was good, the statistical deviation of each measurement encompassing the mean value of the other. The difference between the mean values was 8%.

Dose rates were also measured at four points along the y axis of the crew compartment, and a representative profile of the dose-rate level is shown in Fig. 14.3. A similar profile is given for the dose-rate level at the side of the crew compartment. For these measurements compartment D

[1] For all the measurements reported here, the angle θ was measured in the horizontal plane.

[2] W. F. Hornyak, *Rev. Sci. Instr.* 23, 264 (1952).

[redacted]
2-01-056-3-T6A

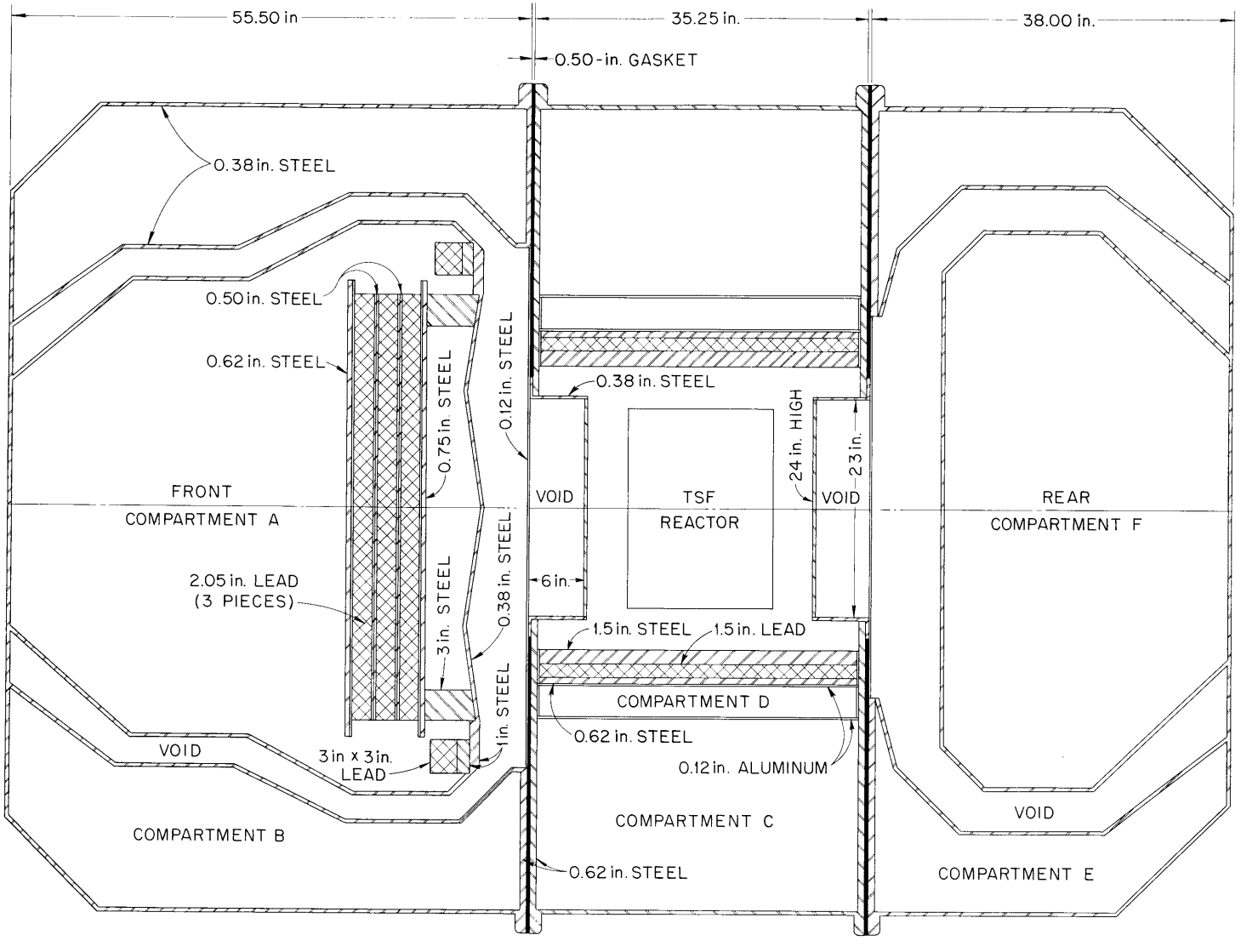

Fig. 14.1. Schematic Diagram of the Mockup of the GE R-1 Reactor Shield.

[redacted] [redacted]

2-01-056-3-T24-81

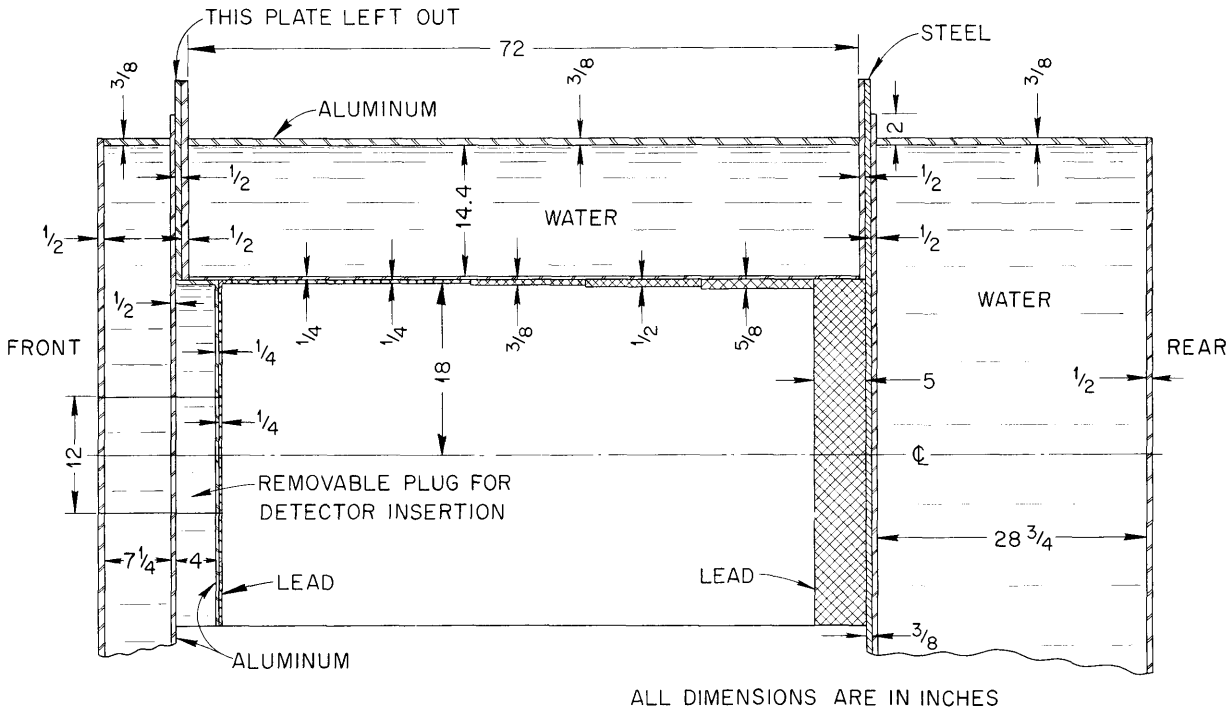

Fig. 14.2. Schematic Diagram of the Mockup of the GE R-1 Crew Compartment.

of the reactor shield (Fig. 14.1) was filled with air, which increased the dose rate by a factor of 1.25 at the center. It is expected that a similar change would be observed at all other points on the profile.

Radiation Measurements in the Crew Compartment as a Function of the Reactor Displacement from the *d* Axis

The G-E Shielding Group has become interested in aircraft configurations in which the reactor and engines may be placed in the wings of the aircraft. Therefore an additional experiment was requested by the G-E group in order to obtain some experimental evidence as to the effect of displacing the reactor shield laterally from the axis of the fuselage.

The gamma-ray dose rate and the neutron flux at the center of the crew compartment were continuously recorded while the reactor shield was moving horizontally a distance of 60 ft along a perpendicular to the usual reactor–crew-compartment axis (*d*). The origin of the perpendicular was on the *d* axis 64 ft from the rear face of the crew compartment. The neutron flux was measured with a BF_3 counter, since the counting rate of the dosimeter is insufficient to operate the automatic-plotting equipment. The gamma-ray dose rate was measured with the standard anthracene scintillation counter.

The results (Figs. 14.4 and 14.5) of this experiment indicate that for a displacement of up to 20 ft the change in dose rate in the crew compartment is not large. The gamma-ray dose rate increased approximately 50%, while the neutron flux remained essentially constant. Beyond 20 ft a rapid change in dose rate was observed. For a 60-ft displacement, the gamma-ray dose rate increased by a factor of 60 and the neutron flux by a factor of 3.6 over the values observed with no displacement. The BF_3 counter, although it does not measure the fast-neutron dose rate directly, was

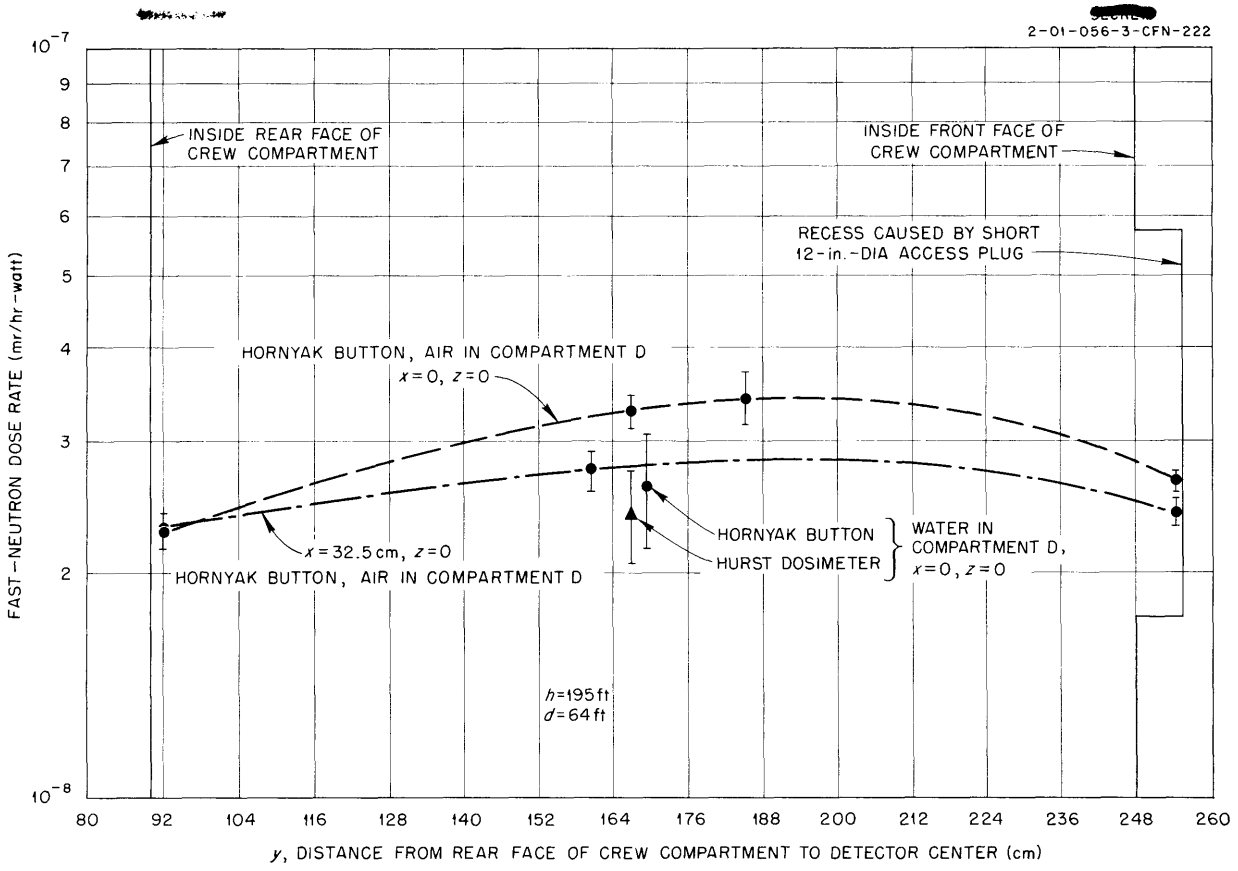

Fig. 14.3. Fast-Neutron Dose Rate as a Function of Position Inside the GE R-1 Crew-Compartment Mockup.

considered to give a reasonably good indication of the relative change in dose rate, since the crew-compartment walls were sufficiently thick for the low- and high-energy neutrons to have reached an equilibrium.

Fast-Neutron Dose-Rate Distribution in Air Around the Reactor Shield

Measurements of the fast-neutron dose rate in air at a considerable distance from the R-1 reactor shield were needed in order to check the calculation of the fast-neutron leakage from the shield and to permit the calculation of the air-scattered dose rate in the crew compartment. It was assumed that the dose rate for the R-1 shield was independent of the azimuthal angle (azimuth about the d axis), and therefore measurements were made only as a function of the horizontal angle θ. The experiment was complicated by the necessity of differentiating between the direct-beam neutrons and those which had been scattered once or more in the air and on the ground. In order to make the differentiation, measurements were made with and without a shadow cone (Fig. 14.6) between the detector and the reactor. All the measurements were made with a Hornyak button.

The measurements without the shadow cone (Fig. 14.7) were made continuously as a function of the distance (up to approximately 11 m) from the center of the reactor to the center of the detector for various angles of θ. In order to delineate the effectiveness of the shadow cone, measurements (Fig. 14.8) were taken with the shadow cone between the reactor and the detector for three values of θ. For these measurements the counter was fixed at approximately 11 m from the center of the reactor, and the shadow cone was moved along the reactor-detector axis from a position adjacent to the detector to a position near the reactor shield.

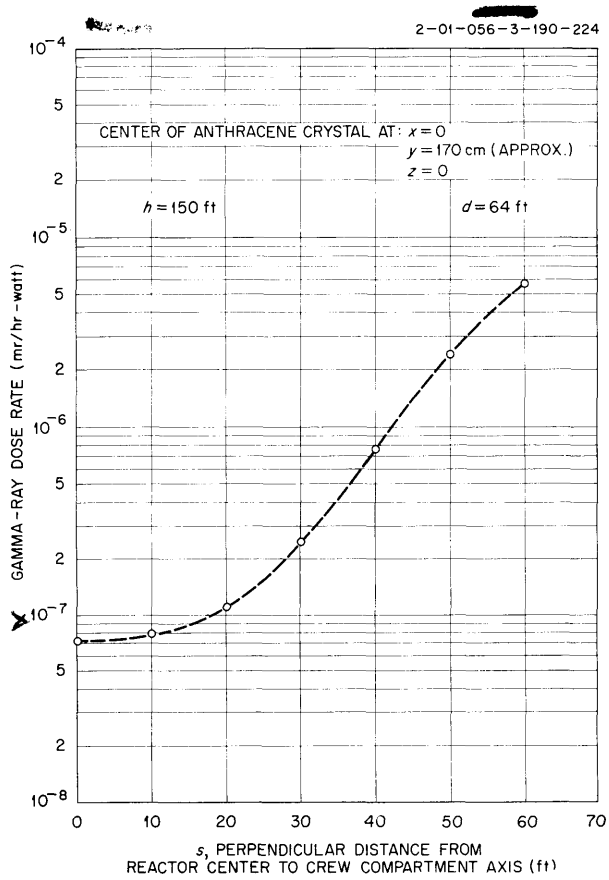

Fig. 14.4. Gamma-Ray Dose Rate near the Center of the GE R-1 Crew Compartment Mockup as a Function of Reactor Displacement from the Crew-Compartment Axis.

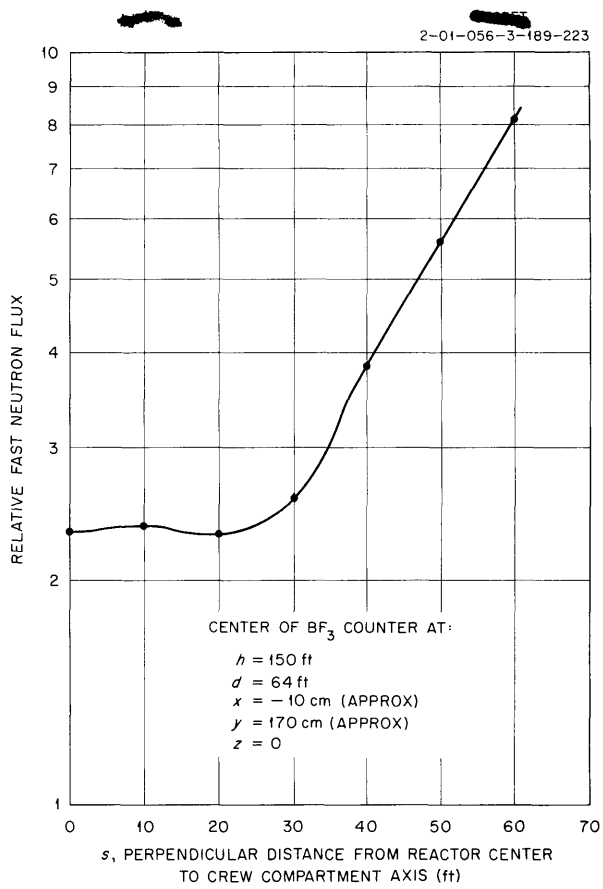

Fig. 14.5. Relative Fast-Neutron Flux near the Center of the GE R-1 Crew Compartment as a Function of the Reactor Displacement from the Crew-Compartment Axis.

Unfortunately, the measurements obtained with the moving shadow cone cannot be interpreted in a reasonably straightforward manner because the finite size of the detector and the semitransparency of the edges of the shadow cone do not allow precise delineation of the geometry for a given position. Further, the geometry of the scattered radiation varies rapidly with changes in θ. These difficulties notwithstanding, it is possible to ascertain a maximum and minimum limit of the air-scattered radiation for each value of θ. The maximum occurs when the solid angle subtended by the reactor shield is equal to the solid angle subtended by the large base of the cone, the solid angle having its origin at the center of the crystal (Fig. 14.9). The minimum occurs when the solid angle subtended by the reactor shield is equal to

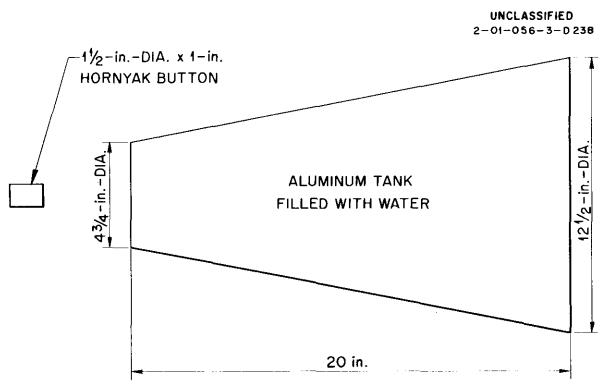

Fig. 14.6. Dimensions of Neutron Shadow Cone and Hornyak Button.

* See errata

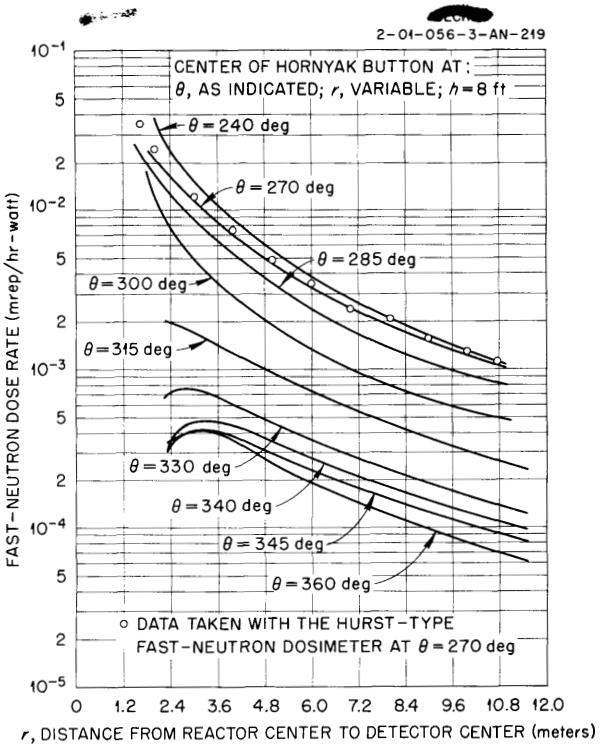

Fig. 14.7. Fast-Neutron Dose Rates as a Function of Distance from the GE R-1 Reactor Shield.

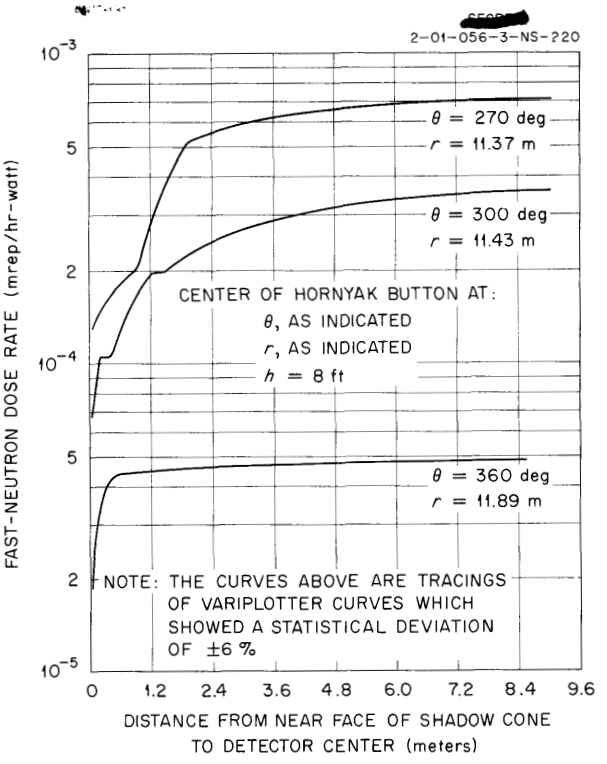

Fig. 14.8. Fast-Neutron Dose Rates as a Function of Shadow-Cone Position Between the GE R-1 Reactor Shield and Detector.

the solid angle subtended by the small base of the shadow cone and is also equal to the solid angle subtended by the detector. The maximum and minimum values obtained for the air-scattered radiation, as well as the maximum direct-beam dose rates obtained for the three angles, are listed in Table 14.1. Since the reactor shield is quite asymmetrical, particularly in the region toward the crew compartment, the direct beam was reduced to less than 25% of the total neutrons in the 360-deg case.

TABLE 14.1. AIR-SCATTERED AND DIRECT-BEAM DOSE RATES AT APPROXIMATELY 11.5 m FROM THE REACTOR FOR VARIOUS VALUES OF θ

θ (deg)	Air-Scattered Dose Rate (mrep/hr·w)		Maximum Direct-Beam Dose Rate (mrep/hr·w)
	Maximum	Minimum	
360	4.5×10^{-5}	4.35×10^{-5}	1.4×10^{-5}
300	1.1×10^{-4}	1.1×10^{-4}	3.4×10^{-4}
270	1.86×10^{-4}	1.55×10^{-4}	7.6×10^{-4}

Neutron Flux in Air as a Function of Distance from the Reactor Shield

There exists a possibility that gamma rays resulting from the capture of neutrons by the air and the ground may be detected in the crew compartment. As a preliminary investigation of the importance of these capture gammas (see the following subsection by F. L. Keller and J. E. Van Hoomissen), the count rate of a fission chamber was observed as a function of distance from the side of the R-1 shield ($\theta = 90$ deg), with and without cadmium covering the center section (compartment C) of the shield. It was necessary to cover only the center section of the shield because all the other sections contained borated (1 wt % boron) water. The presence of the cadmium reduced the intensity of the count rate by approximately 30% and apparently did not change the shape of the curve (Fig. 14.10). The measurement was then made with the entire shield covered with

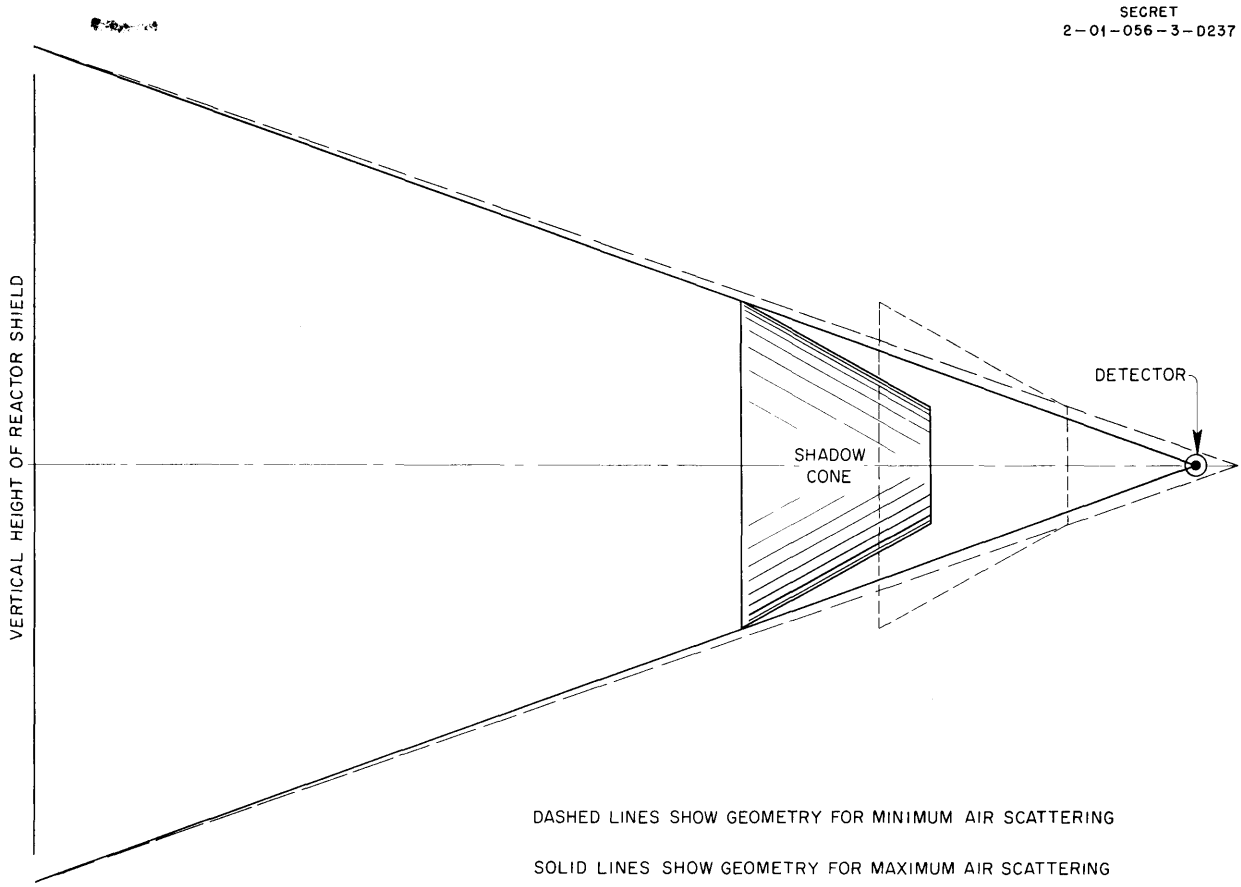

Fig. 14.9. Geometry for Shadow-Cone Experiment with the GE R-1 Reactor Shield.

cadmium. The presence of the cadmium again reduced the count rate by approximately 30%. Results of this experiment indicate that boration of the hydrogenous shielding effectively eliminates the low-energy component of the neutron spectrum; therefore the only effective way of reducing capture gamma rays in air is by further addition of hydrogenous shielding.

TSF Reactor Power Determination

A calorimetric determination of the power level of the TSF reactor made at the completion of these G-E experiments indicated a 20% increase in power during the course of the experiments. The reason for this discrepancy has not been ascertained.

[3]Boeing Airplane Company.

CALCULATION OF THE CONTRIBUTION OF GAMMA RAYS FROM NEUTRON CAPTURES IN AIR TO THE GAMMA-RAY DOSE RATE INSIDE THE G-E CREW-SHIELD MOCKUP

F. L. Keller J. E. Van Hoomissen[3]

The measured gamma-ray dose rate minus the calculated direct-beam dose rate in the G-E crew compartment with the TSF reactor encased in the GE R-1 mockup was found[4] to differ by a factor of 16 from the calculated dose rate expected from air-scattered gamma rays. This discrepancy prompted an investigation to determine whether secondary gamma rays produced by air captures of neutrons would account for a large part of the difficulty.

[4]*Engineering Progress Report No. 17*, APEX-17 (Sept. 1955), p 124.

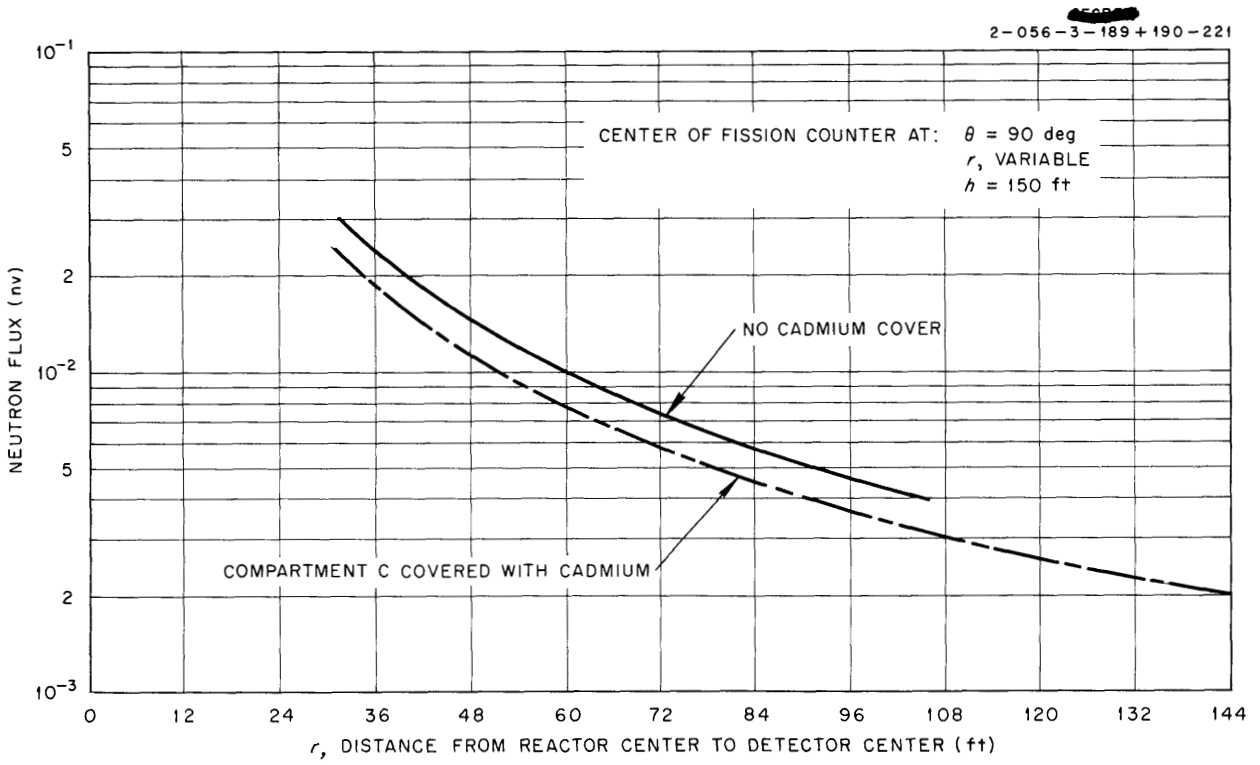

Fig. 14.10. Neutron Flux in Air as a Function of Distance from GE R-1 Reactor Shield.

Determination of "Effective Thermal-Neutron Flux"

In order to carry out a calculation of the gamma-ray dose-rate contribution expected from neutron captures in air, it was first necessary to determine the "effective thermal-neutron flux" outside the R-1 reactor shield. To do this, fission-counter measurements of the flux were taken at the side of the shield (see the preceding subsection by F. N. Watson). The results of these measurements, which consisted of a radial traverse from 30 to 140 ft at the side of the R-1 shield (θ = 90 deg), are shown in Fig. 14.10. The fission counter was calibrated with a thermal-neutron source. Thus, if the uranium fission cross section varied as approximately $1/v$ in the region of interest,[5] the measurement gave an effective thermal-neutron flux which, when multiplied by the macroscopic thermal-absorption cross section for a reaction involving any other $1/v$ absorber, gave the rate of absorption per unit volume for that reaction.

[5]Other measurements with a BF_3 proportional counter show essentially the same capture rate and confirm the validity of this premise for the present application.

This measured effective thermal-neutron flux was fitted with an analytical expression of the form

$$\phi = \frac{A\, e^{-Kr}}{r}\,, \tag{1}$$

where

A = 26.3 neutrons/cm^2-sec-watt,
K = 1.56×10^{-4} cm^{-1},
r = distance from the center of the reactor to the detector (cm).

The expression fits the experimental curve very well in the region covered by the measurements and has the form of the solution to the diffusion equation, which should hold at larger distances. In the calculation it was assumed that the effective thermal-neutron flux around the R-1 shield was isotropic in angle and had the radial dependence given by Eq. 1. Subsequent measurements have shown that the flux at the front of the shield (θ = 0 deg) for $r \sim 100$ ft is only about one-half the value given by this expression. However, since the flux is expected to be lowest in the

forward direction, it is felt that the error involved in using Eq. 1 for the flux, at any point, from the R-1 shield does not affect the final result by more than about 25%.

Calculation of Capture-Gamma-Ray Dose Rate

The calculation of the capture-gamma-ray dose rate was accomplished in two parts. For the first part a geometry (Fig. 14.11) was used in which the reactor and R-1 shield were replaced by a point isotropic source at S, where the effective thermal-neutron flux originates. The differential gamma-ray dose rate at P, that is, the dose rate at P from capture gamma rays arriving at P in the conical shell between the angles β and $\beta + d\beta$, was then calculated as a function of the angle β. In the second part of the calculation the point P was placed at the center of the G-E crew compartment. The dose rate at this point was then determined by weighting the angular distribution obtained from the first part of the calculation with attenuation and buildup factors corresponding to slant penetrations through the crew-compartment shielding.

[redacted]
2-01-056-3-D233

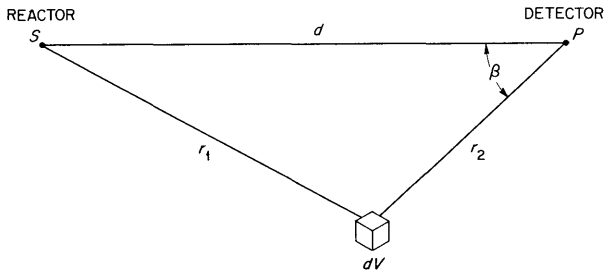

Fig. 14.11. Geometry for the Calculation of the Capture-Gamma-Ray Dose Rate in the GE R-1 Crew Compartment.

Dose Rate at a Point in Space from Air-Capture Gamma Rays. – Oxygen has a negligible thermal-absorption cross section for the (n,γ) reaction, and therefore all the air-capture gamma rays were assumed to be produced in nitrogen. The microscopic thermal-absorption cross section for nitrogen, $\sigma_N(n,\gamma)$, is 0.1 barn, and thus the macroscopic cross section, $\Sigma_N(n,\gamma)$, for this reaction is 4.13×10^{-6} cm^{-1}. The absorption cross section for nitrogen is expected to vary as $1/v$, and therefore the rate of (n,γ) absorptions that take place in an element of volume dV is given by $\phi\Sigma_N\, dV$, where ϕ is the "effective thermal-neutron flux" given by Eq. 1. On the average, there are 1.7 gamma rays with a total energy of 10.8 Mev produced per absorption in nitrogen. Of these, 90% have energies between 5 and 7 Mev. Thus, for the purpose of this calculation, it was assumed that 1.7 gamma rays of energy 6 Mev were produced per absorption. The number of gamma rays produced per second per watt in the element of volume dV was then given by $1.7\phi\Sigma_N\, dV$.

Since the capture gamma rays are emitted isotropically, the number of gamma rays arriving at a unit detector at the point P per second per watt from the element of volume dV is given by

$$(2) \qquad \frac{1.7\phi\Sigma_N\, e^{-\mu r_2}}{4\pi r_2^2}\, dV ,$$

where

μ = linear absorption coefficient of air for 6-Mev gamma rays,

r_2 = distance from the element of volume dV to P (cm).

The total number of gamma rays arriving at the unit detector at P per second per watt is then given by

$$(3) \qquad \frac{1.7A\Sigma_N}{4\pi} \iiint \frac{e^{-Kr_1}\, e^{-\mu r_2}}{r_1 r_2^2}\, r_2^2 \sin\beta\, d\beta\, d\phi\, dr_2 ,$$

where

$$r_1 = (r_2^2 + d^2 - 2r_2 d \cos\beta)^{1/2} .$$

The total dose rate per watt measured at the detector, D_p, is obtained by multiplying Eq. 3 by ϵ, the factor for converting gamma rays per square centimeter per second to dose rate for 6-Mev gamma rays. After integrating over ϕ, this gives

$$(4) \qquad D_p = 0.85A\Sigma_N\epsilon \int_0^{\pi}\int_0^{\infty} \frac{e^{-\mu r_2}\, e^{-K(r_2^2 + d^2 - 2r_2 d\cos\beta)^{1/2}}}{(r_2^2 + d^2 - 2r_2 d\cos\beta)^{1/2}} \sin\beta\, dr_2\, d\beta = \int_0^{\pi} M(\beta)\, d\beta ,$$

where

$$M(\beta) = 0.85 A \Sigma_N \epsilon \int_0^\infty \frac{e^{-\mu r_2} e^{-K(r_2^2 + d^2 - 2r_2 d \cos\beta)^{1/2}}}{(r_2^2 + d^2 - 2r_2 d \cos\beta)^{1/2}} \sin\beta \, dr_2 \, . \tag{5}$$

The expression $M(\beta)\, d\beta$ gives the dose rate per watt at P produced by gamma rays arriving in the conical shell between the angles β and $\beta + d\beta$; $M(\beta)$ was determined by numerically integrating the expression in Eq. 5 for various values of β. The constants used in these integrations were:

A = 26.3 neutrons/cm^2-sec-watt,
$K = 1.56 \times 10^{-4}$ cm^{-1},
$\mu = 3.04 \times 10^{-5}$ cm^{-1},
$d = 1.98 \times 10^3$ cm (65 ft),
$\epsilon = 6.72 \times 10^{-3}$ (mr/hr)/(gamma rays/cm^2·sec).

The result of the integration is shown in Fig. 14.12. The area under the curve represents the total gamma-ray dose rate in air at the point P. The value of the integral is 1.85×10^{-6} mr/hr-watt. From Fig. 14.12 it may be seen that the maximum contribution comes from gamma rays entering at approximately 50 deg to the reactor-detector axis (see Fig. 14.11).

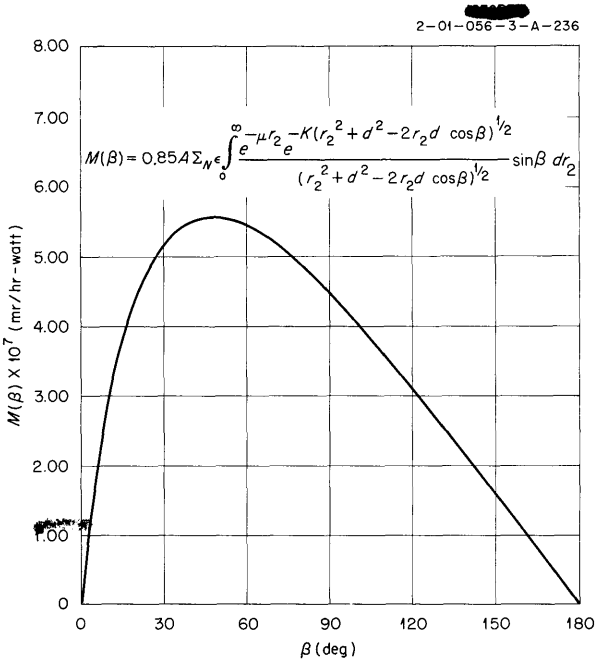

Fig. 14.12. Capture-Gamma-Ray Dose Rate at a Point 64 ft from the GE R-1 Reactor Shield as a Function of the Angle of Incidence of the Capture Gamma Rays.

Dose Rate at the Center of the Crew Compartment from Air-Capture Gamma Rays. – The point P was placed at the center of the G-E crew compartment as shown in Fig. 14.13. The dose rate expected at the center of the crew compartment, D_{cs}, was then obtained by weighting each point of the curve given in Fig. 14.12 by the attenuation factor corresponding to the proper slant distance through the shield for that particular angle and integrating under the resulting curve. Thus

$$D_{cs} = \int M(\beta)\, B_1\left(\frac{\mu_{H_2O} t_{H_2O}}{\sin\beta}\right) e^{-\mu_{H_2O} t_{H_2O}/\sin\beta}\, B_2\left(\frac{\mu_{Pb} t_{Pb}}{\sin\beta}\right) e^{-\mu_{Pb} t_{Pb}/\sin\beta} = \int G(\beta)\, d\beta \, , \tag{6}$$

where

μ_{H_2O}, μ_{Pb} = linear absorption coefficients for 6-Mev gamma rays in water and lead, respectively,

$B_1\left(\frac{\mu_{H_2O} t_{H_2O}}{\sin\beta}\right)$, $B_2\left(\frac{\mu_{Pb} t_{Pb}}{\sin\beta}\right)$ = dose buildup factors for plane monodirectional 6-Mev gamma rays in water and lead, respectively.

[redacted]

[redacted]

2-01-056-3-D234

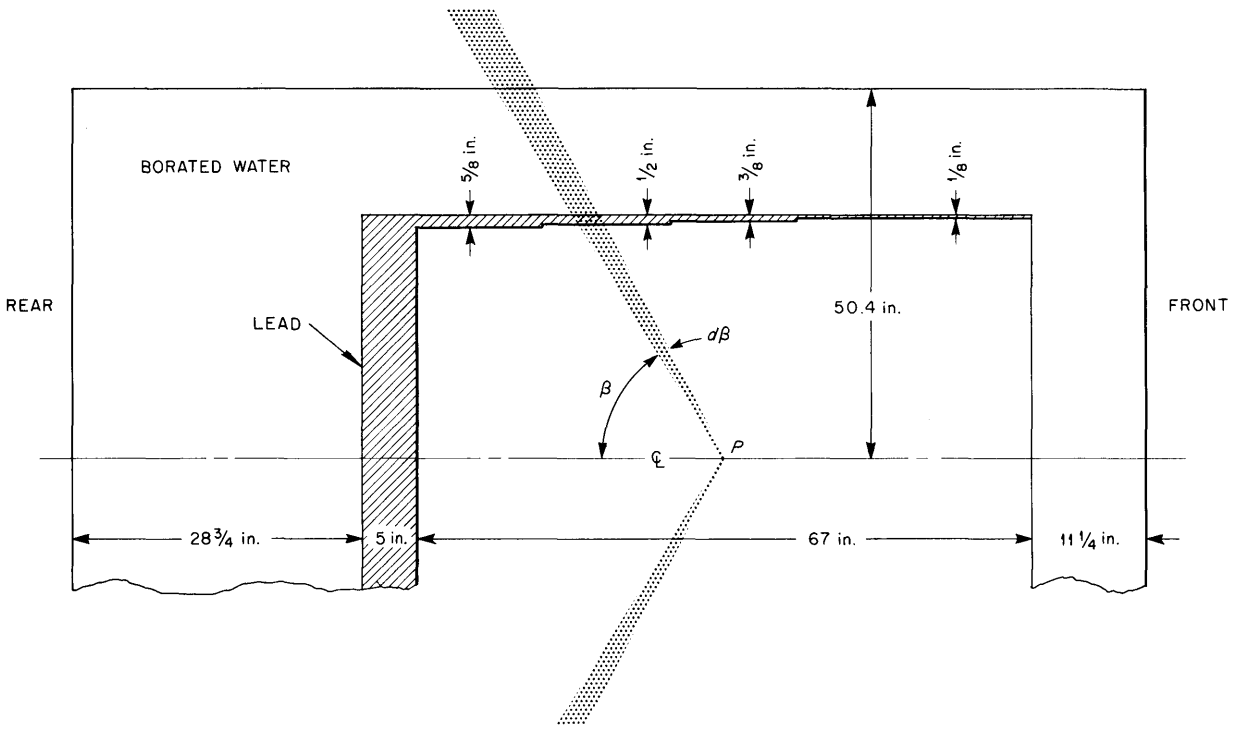

Fig. 14.13. Mockup Thicknesses Used for Calculating the Slant Penetration of Capture Gamma Rays in the GE R-1 Crew Compartment.

This calculation was carried out only for 30 deg $< \beta <$ 150 deg. This range of angles covered the entire side of the crew shield but omitted the front and the rear. It was also assumed that gamma rays which entered the side of the shield at a given angle with respect to the surface continued through the shield at this same angle with only a change in intensity as a result of attenuation and buildup. The scattering that takes place in the shield was neglected, and hence an angular distribution was assigned to the radiation at the inside surface of the shield. If the crew compartment is of uniform thickness and infinite in length, an integration over the entire shield, for any angular distribution, yields the same value for the dose rate at a point from radiation which entered the shield at a given angle as that obtained by the method used above. For a shield of finite length, however, the method used above gives a slightly high value for the dose rate from radiation entering at a particular angle. Thus the calculated contribution from radiation which entered the side of the G-E shield at angles between 30 and 150 deg should be slightly high. However, in the calculation described above, the radiation which approached the side of the shield at angles from 0 to 30 deg and from 150 to 180 deg was neglected. The gamma rays cannot enter the side and then reach the center of the compartment along a straight-line path at these angles, but, because of scattering in the shield, many of them, nevertheless, actually reach the center. For this reason it is believed that the omitted dose-rate contributions mentioned above approximately compensate for the slight overestimate of the dose-rate contribution from gamma rays which entered the side at angles between 30 and 150 deg. The dose-rate contribution from capture gamma rays which enter through the rear of the crew shield should be negligible because of the 5 in. of lead at the rear of the crew compartment.

A plot of the integrand of Eq. 6 vs β is shown in Fig. 14.14. The discontinuities in the curve are caused by abrupt changes in the lead thickness at the side of the crew compartment. From this curve it may be seen that the attenuation

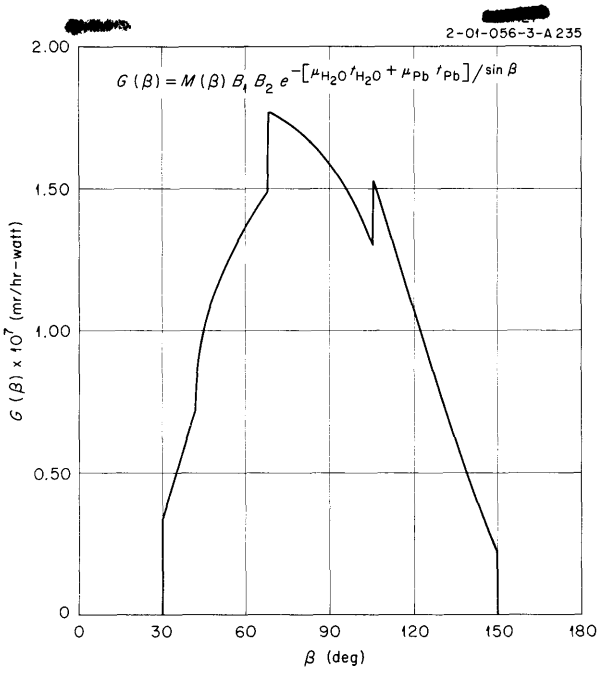

Fig. 14.14. Capture-Gamma-Ray Dose Rate at the Center of the GE R-1 Crew Compartment as a Function of the Angle of Incidence of the Capture Gamma Rays.

through the side of the crew compartment shifts the maximum contribution of dose rate to the gamma rays which enter the crew compartment at approximately 80 deg from the reactor–crew-compartment axis. Again, the area under this curve gives the dose rate at the center of the crew compartment from air-capture gamma rays as approximately 4×10^{-7} mr/hr-watt. The measured gamma-ray dose rate at the center of the crew compartment was 7×10^{-7} mr/hr-watt. The calculated direct-beam dose rate is 6.6×10^{-8} mr/hr-watt, and the calculated air-scattered gamma-ray dose rate is only 3.9×10^{-8} mr/hr-watt. Thus it does appear that the gamma rays from air capture of neutrons may account for a large part of the dose rate measured inside the G-E crew shield.

Other sources which may contribute to the measured dose rate at the center of the crew compartment are: gamma rays from neutron captures by the hydrogen and boron in the crew shield; gamma rays from inelastic scattering of neutrons in air; gamma rays resulting from the decay of unstable nuclei formed in other neutron reactions in air, such as the fast-neutron (n,p) reaction in oxygen, which gives N^{16} decaying with a 6-Mev gamma ray; and multiply air-scattered gamma rays. The contribution from captures in the crew compartment has been estimated to be approximately 1×10^{-7} mr/hr-watt. The other possible sources mentioned above are being investigated further.

APPLICATION OF DIFFERENTIAL SHIELDING EXPERIMENTS TO PREDICT NEUTRON DOSE RATE IN THE GE R-1 CREW-SHIELD MOCKUP

G. J. Rausa

A calculation of the fast-neutron dose rate at the center of the G-E crew-compartment mockup has been made for comparison with experimental data. The calculation utilized modified scattering probabilities[6] derived from data obtained during the differential shielding experiments and the fast-neutron dose-rate measurements in air around the R-1 reactor shield. An attempt was also made to calculate the dose measured in the side of the detector tank as a function of effective water thickness.

Determination of Direct Radiation Around R-1 Mockup

The direct-beam dose rate, D_d, around the reactor shield was determined from experimental measurements of the total dose rate, D_T, and the scattered dose rate, D_s (reported in a preceding subsection, "GE R-1 Divided Shield Mockup Experiments"). Measurements with an unshielded detector (Fig. 14.7) gave the total dose rate as a function of the emission angle θ and the radial distance from the reactor. Measurements with a shadow cone between the reactor and detector (Figs. 14.6 and 14.8) gave the scattered dose for three values of θ (270, 300, and 360 deg) at a fixed radial distance. Since the measured value of the scattered contribution varies with the position of the shadow cone, the values of the scattered radiation used in the calculation were averages of the minimum and maximum values shown in Table 14.1. When these shadow-cone measurements are used, radiation scattered at low angles must be considered as part of the direct dose. The direct dose is assumed to be the difference between D_T and D_s measured at the same point. It was then assumed that D_d follows the inverse square law out to 64 ft. Since D_s was measured

[6] M. F. Valerino, *ANP Quar. Prog. Rep. June 10, 1955*, ORNL-1896, p 206.

only for $\theta = 270$, 300, and 360 deg, it was necessary [redacted] consider the following assumptions with regard to D_s for the region 180 deg $< \theta <$ 270 deg:

1. $D_s(\theta) = 0.19 D_T(\theta)$. This assumption was based on the ratio D_s/D_T for $\theta = 270$, 300, and 360 deg being 0.19, 0.24, and 0.75, respectively. Since the reactor shielding is approximately the same for θ = 180 to 270 deg, the smaller fraction of the total dose was assumed.
2. $D_s(\theta)$ is symmetrical about $\theta = 270$ deg. This assumption represents an extreme case.
3. $D_s(\theta)$ is a constant and equals D_s(270 deg). This assumption also represents an extreme case.

The effect of these three assumptions on the total dose rate at a distance of 64 ft is shown in Fig. 14.15.

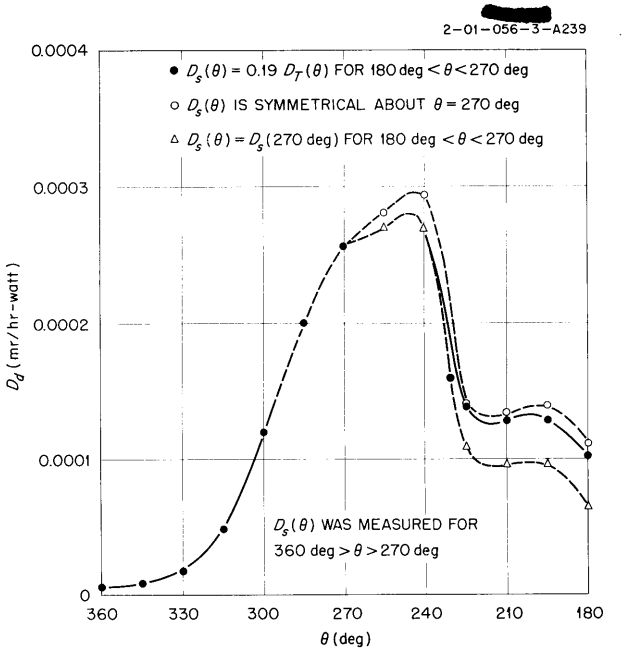

Fig. 14.15. Effect of Various Assumptions on the Direct-Beam Dose Rate as a Function of θ.

Calculation of the Crew-Compartment Dose Rate

The direct dose used in the calculation was that obtained under assumption 1 above. Actually, the calculations show that the contributions to the scattered dose for 240 deg $< \theta <$ 360 deg account for 96% of the total scattered dose; thus the dependence of $D_s(\theta)$ on any of the three assumptions for 180 deg $< \theta <$ 240 deg is small. It should also be remembered that D_d(360 deg) was obtained from the difference between large numbers, and therefore this determination is not so accurate as that for D_d in the vicinity of $\theta = 270$ deg, where the scattered dose makes a small contribution to the total dose.

The dose was calculated for each of 12 conical segments, with the shield thickness, T_n, taken to be constant over each segment, by using the following equations[7] (refer to Fig. 14.16 for the geometry):

$$D_s^s = \sum_{n=1}^{N} (\cos\theta_n'' - \cos\theta_n')\, D_d(a,\ell)\, e^{-\int_0^{T_n} dt/\lambda_d}\, \ell^2 P_s^s(\theta_n)\, f_s^s\, e^{-\int_0^{T_s} dx/\lambda_s^s} ,$$

where

θ_n'', θ_n, θ_n' = initial, middle, and final angle of the nth interval, as defined in Fig. 14.16,

$D_d(a,\ell)\, e^{-\int_0^{T_n} dt/\lambda_d}$ = direct-beam dose, $D_d(\theta)$,

ℓ = distance from center of the reactor to the rear face of the crew compartment,

T_n = thickness of neutron shield at the reactor,

λ_d = relaxation length of the direct beam in the neutron shield,

$P_s^s(\theta_n)$ = probability of scattering into the side of the crew compartment for $T_s = 0$ and for the nth conical beam segment,

T_s = thickness of neutron shield at the side of the crew compartment,

f_s^s = focusing factor for side-scattered radiation,

$e^{-\int_0^{T_s} dx/\lambda_s^s}$ = attenuation of radiation scattered into the side of the crew compartment (T_s = 37.5 cm),

λ_s^s = relaxation length for the scattered dose in the side of the crew compartment.

[7] M. F. Valerino and F. L. Keller, *ANP Quar. Prog. Rep. Sept. 10, 1955*, ORNL-1947, p 205.

[redacted]

[redacted]
2-01-056-3-D240

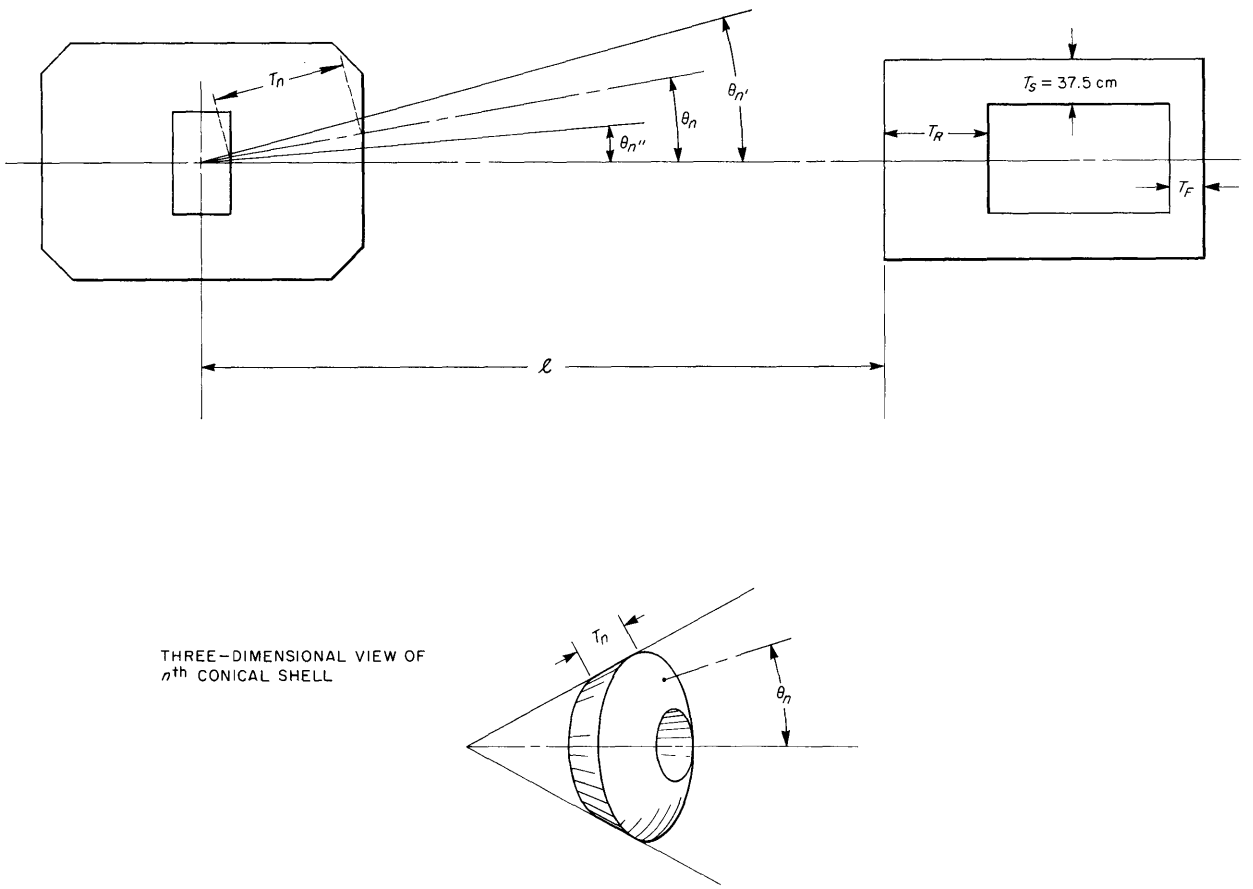

Fig. 14.16. Geometry Used for Calculation of Neutron Dose Rate in GE R-1 Crew Compartment.

The effective value of T_n was determined from a graph of the known $D_d(\theta)$ vs T_n. The λ_d for each T_n was obtained from a graph of λ_d vs T_n published previously.[6,7] The λ_s^s was computed by using the relation[7]

$$\lambda_s^s(T_n,T_s) = \frac{\lambda_s^s(45,T_s)}{\lambda_d(45+T_s)}\,\lambda_d(T_n+T_s) \ .$$

The function

$$\ell^2 P_s^s(\theta)\, e^{-\int_0^{T_s} dx/\lambda_s^s} \ ,$$

for T_s = 37.5 cm, was then generated (Fig. 14.17).

The scattered-dose-rate contributions from each conical shell are plotted as a function of θ in Fig. 14.18. The calculated total scattered dose rate was 7.5×10^{-8} mrep/hr-watt. The direct dose was estimated to be 0.5×10^{-8} mrep/hr-watt, at most, and therefore the calculated total dose rate at the center of the crew compartment was about 8×10^{-8} mrep/hr-watt. The measured dose rate was found to be 2.5×10^{-8} mrep/hr-watt, and thus the calculated rate was an overestimate by a factor of 3.2. The calculation did not take into account the ducts, which would give rise to radiation that, in penetrating the crew compartment, would have a relaxation length shorter than that used in the calculation. Part of this discrepancy is, in all probability, due to the assumption of cylindrical symmetry for the R-1 shield, which is not quite true.

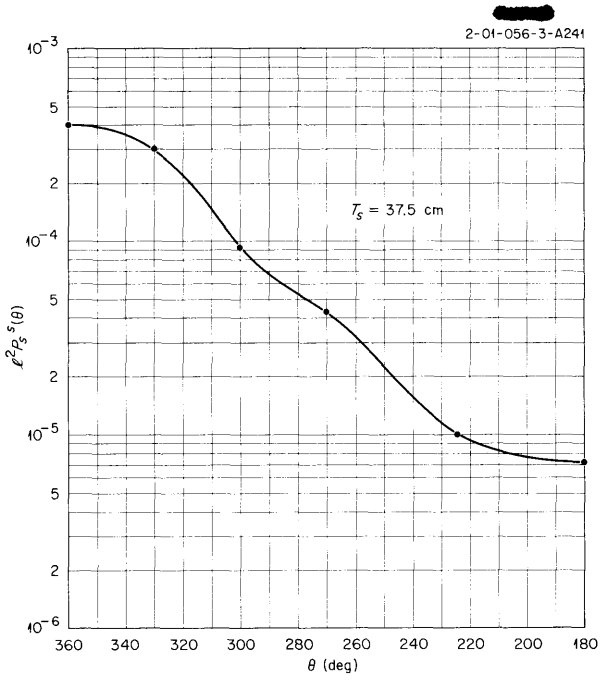

Fig. 14.17. Neutron Scattering Probability from a Conical Shell Beam – Reactor Encased in GE R-1 Shield.

Calculation of Scattered Dose Rate in the Detector Tank

In view of the discrepancy between the calculated and measured crew-compartment dose rates, as mentioned above, an attempt was made to calculate the scattered fast-neutron dose rate in the detector tank as a function of the effective water thickness. A comparison of the calculations and the measured data (Fig. 14.19) indicates that the relaxation lengths λ_s^s used for the calculation were somewhat longer than the actual relaxation lengths. The calculated value for T_s varies from a factor of 1.3 to 2.3 higher than the measured value in the range of 8 to 37.5 cm. Extrapolation of both curves to $T_s = 0$ indicates that the calculated dose rate at the surface would be very close to the measured dose rate. From the foregoing information, it might be inferred that the radiation was "softer" than was assumed in the calculations and that the difference in the radiation could be due to neglecting the ducts. Also, the focusing factor used in the calculation may have been high by a factor of up to 1.4.

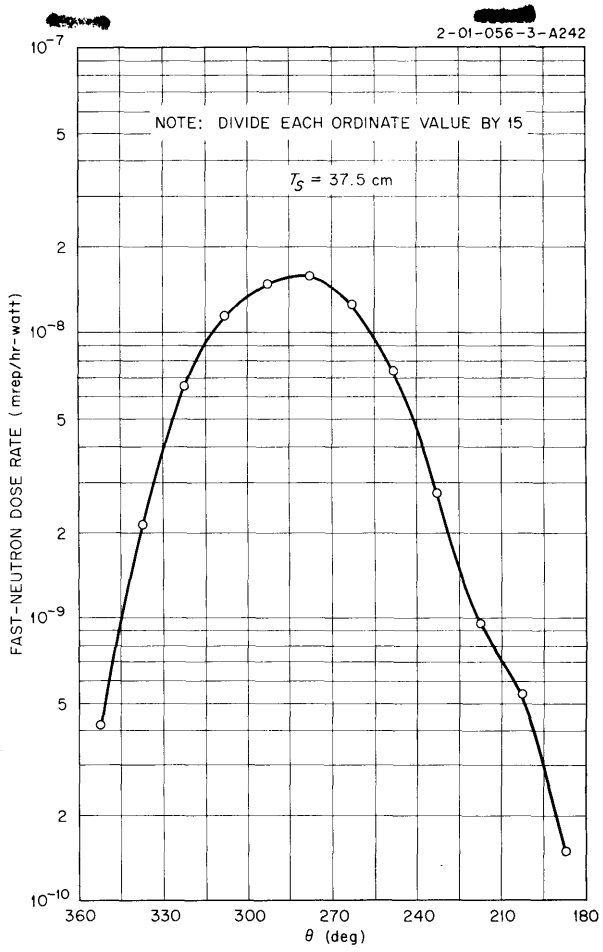

Fig. 14.18. Fast-Neutron Dose Rate Scattered into Side of GE R-1 Crew-Compartment Mockup as a Function of Reactor Angle θ.

PROCEDURE FOR THE OPTIMIZATION OF A UNIT NEUTRON SHIELD

G. J. Rausa

In some aircraft applications it is conceivable that a unit neutron shield will be required, and it will, of course, be necessary to minimize the shield weight in order to obtain optimum over-all performance. The optimization procedure for the unit shield is simpler than that for the divided shield[8] because of the fewer number of variables. The procedure consists in expressing both the

[8] M. F. Valerino and F. L. Keller, *ANP Quar. Prog. Rep. Sept. 10, 1955*, ORNL-1947, p 205; see also Fig. 14.16, this report, for similar geometry.

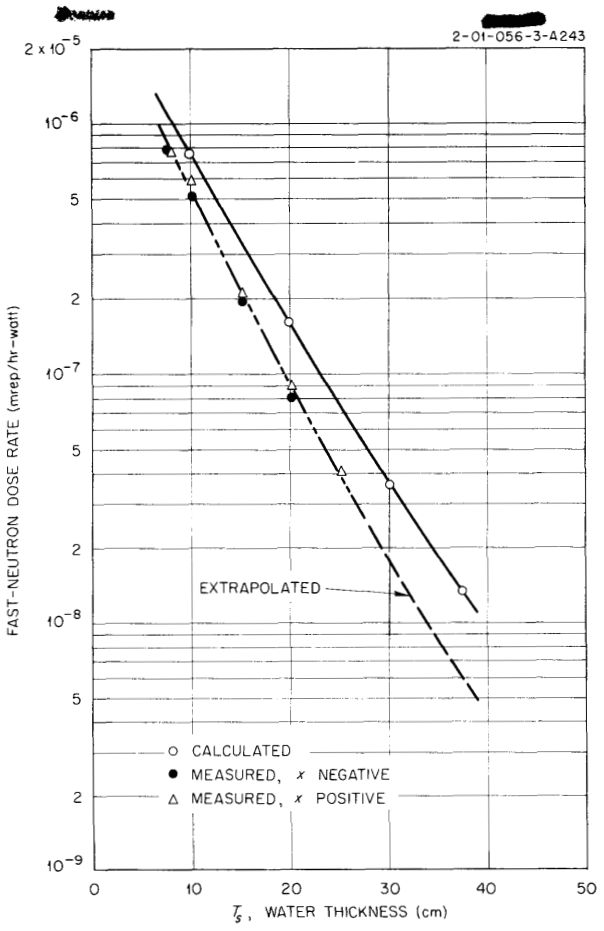

Fig. 14.19. Fast-Neutron Dose Rate as a Function of Effective Water Thickness Along x Axis of the TSF Detector Tank.

weight of the shield and the dose as a function of reactor shield thickness and applying the method of Lagrange multipliers to obtain extremital values.

[redacted] Determination of Shield Weight

Since there is no crew compartment to consider, the total weight of the neutron shield is that of the neutron shield required by the reactor assembly. As was previously outlined in the optimization procedure for the divided shield,[8] the reactor shield assembly is divided into N conical shells, with the weight of each shell being

$$W_n = \frac{2\pi\rho}{3}\,(R_n^3 - a^3)\,\Delta\cos\theta_n \ , \tag{1}$$

where

R_n = outer radius of the shield for the nth shell
= $T_n + a$,
T_n = thickness of hydrogenous neutron shielding,
a = outer radius of reactor core plus 6 in. of lead shielding (79.4 cm),
ρ = density of neutron shielding material,
$\Delta\cos\theta_n$ = $\cos\theta_n'' - \cos\theta_n'$,
θ_n'', θ_n, θ_n' = initial, middle, and final angles of the nth interval, respectively.

The total shield weight for N conical sections is

$$W_T = \Sigma\, W_n \ . \tag{2}$$

Calculation of Dose Rates

The dose rate at a given distance from the reactor shield assembly is made up of both direct and scattered radiation. The scattered-dose-rate contribution from the nth conical shell can be written as

$$D_n^s = \int_{\cos\theta_n'}^{\cos\theta_n''} D_d'\, P_n^s(\theta)\, d(\cos\theta) \ , \tag{3}$$

where

$$D_d' = \ell^2 D_d(a,\ell)\, e^{-\int_0^{T_n} dt/\lambda_d} ,$$

$D_d(a,\ell)\, e^{-\int_0^{T_n} dt/\lambda_d}$ = direct-beam dose rate at ℓ, as determined from LTSF measurements and proper transformations (Fig. 14.20),
ℓ = distance from center of reactor to the point at which the dose rate is determined = 41 ft,
$\lambda_d(T_n)$ = relaxation length of the direct beam in the neutron shield,
$P_n^s(\theta)$ = neutron scattering probability determined from TSF data.

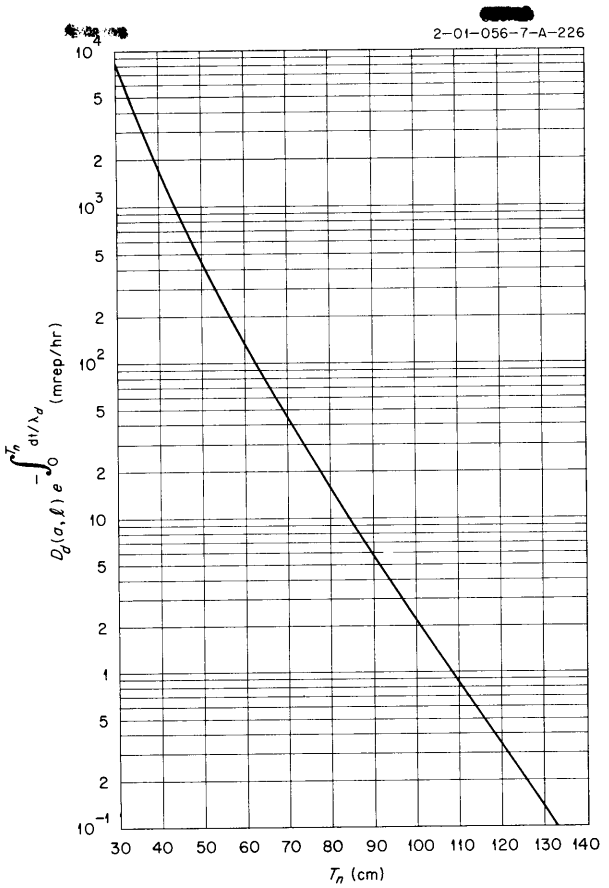

Fig. 14.20. Direct Neutron Dose Rate as a Function of Neutron Shield Thickness.

The values of $\lambda_d(T_n)$ (Fig. 14.21) were determined by applying transformations to LTSF measurements for a CFR mockup with a 6-in.-thick lead shield. Comparison of these values with measured values from TSF data show that for large values of T_n the relaxation lengths approach each other but that for small values of T_n the relaxation lengths are dependent upon the thickness of material preceding the hydrogenous absorber.

The values of $P_n^s(\theta)$ used in this report result from extrapolations of measurements in the TSF detector tank to the surface of the tank. The extrapolated value was multiplied by 2 to take into account the total solid angle and by $^{64}/_{41}$ to correct for the difference in ℓ (measurements were taken for ℓ = 64 ft). The function $\ell^2 P_n^s(\theta)$ is plotted in Fig. 14.22 for ℓ = 41 ft and an altitude of 1200 ft.

The direct-beam dose-rate contribution from each conical shell was shown previously[8] to be

$$(4)\quad D_n^d = \Delta \cos^{m+1}\theta_n\, D(a,\ell)\, e^{-\int_0^{T_n} dt/\lambda_d} ,$$

for $0 < \theta < 90$ deg, if the radiation at the surface of the shield is assumed to have a $\cos^m \theta$ distribution. The total dose rate therefore is

$$(5)\qquad D_T = \sum_{n=1}^{N} D_n^d + D_n^s .$$

Application of Lagrange Multipliers

The method of Lagrange multipliers is used to minimize the shield weight; thus

$$(6)\quad \frac{\partial W_T}{\partial T_n} = -\frac{1}{L_n}\frac{\partial D_T}{\partial T_n} , \qquad n = 1, \ldots, N ,$$

or

$$L_n = -\frac{\partial D_T/\partial T_n}{\partial W_T/\partial T_n} .$$

Substituting Eqs. 1 and 5 in Eq. 6 yields

$$(7)\qquad L_n = \frac{(D_n^d + D_n^s)/\lambda_d(T_n)}{2\pi\rho\,\Delta\cos\theta_n\, R_n^2} ,$$

but

$$D_n^d + D_n^s = D_d(a,\ell)\, e^{-\int_0^{T_n} dt/\lambda_d}\,[\cos^{m+1}\theta_n + \cos\theta_n\, \ell^2 P^s(\theta_n)] ,$$

in which case

$$(8)\qquad 2\pi\rho L_n = \frac{D_d(a,\ell)\, e^{-\int_0^{T_n} dt/\lambda_d}}{\lambda_d(T_n)\, R_n^2}\; \ell^2 P^s(\theta)_n + \frac{\Delta\cos^{m+1}\theta_n}{\Delta\cos\theta_n} .$$

[redacted]

[redacted]

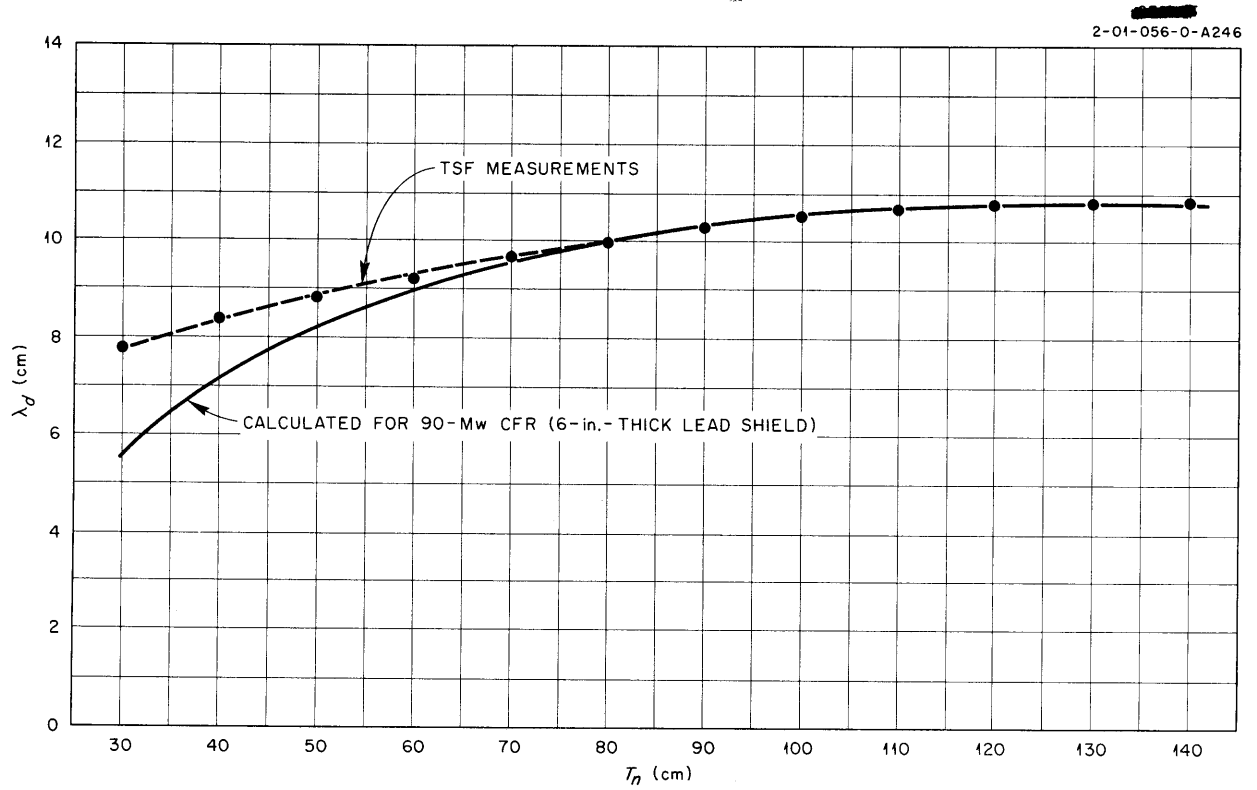

Fig. 14.21. Comparison of Direct-Beam Relaxation Lengths.

[redacted]

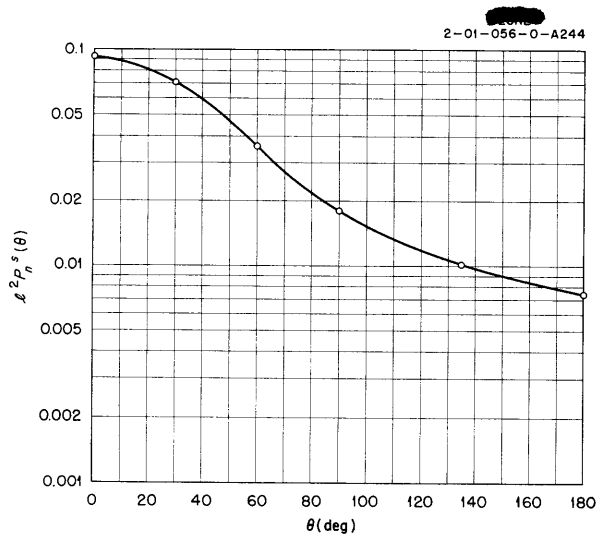

Fig. 14.22. Scattering Probability as a Function of θ for ℓ = 41 ft.

A plot of Eq. 8 for a 90-Mw power level and an assumed $\cos^{10}\theta$ distribution at the shield surface is shown in Fig. 14.23. The optimum unit-shield shape is immediately defined by choosing a Lagrange multiplier.

A few values of the total dose rates and corresponding weights of neutron shielding (ρ = 1 g/cm^3) have been computed (Table 14.2). For $2\pi L = 2.5 \times 10^{-6}$, the values of R_n for 15-deg intervals in θ are listed in Table 14.3.

It may be seen from Eq. 8 that the assumption concerning the angular distribution of radiation leaving the surface of the shield essentially dictates the shape of the shield for $0 < \theta < 90$ deg and that altitude determines the shape for 90 deg $< \theta <$ 180 deg. Other calculations should be carried out in order to determine the effect of the assumed distribution on the weight of the shield.

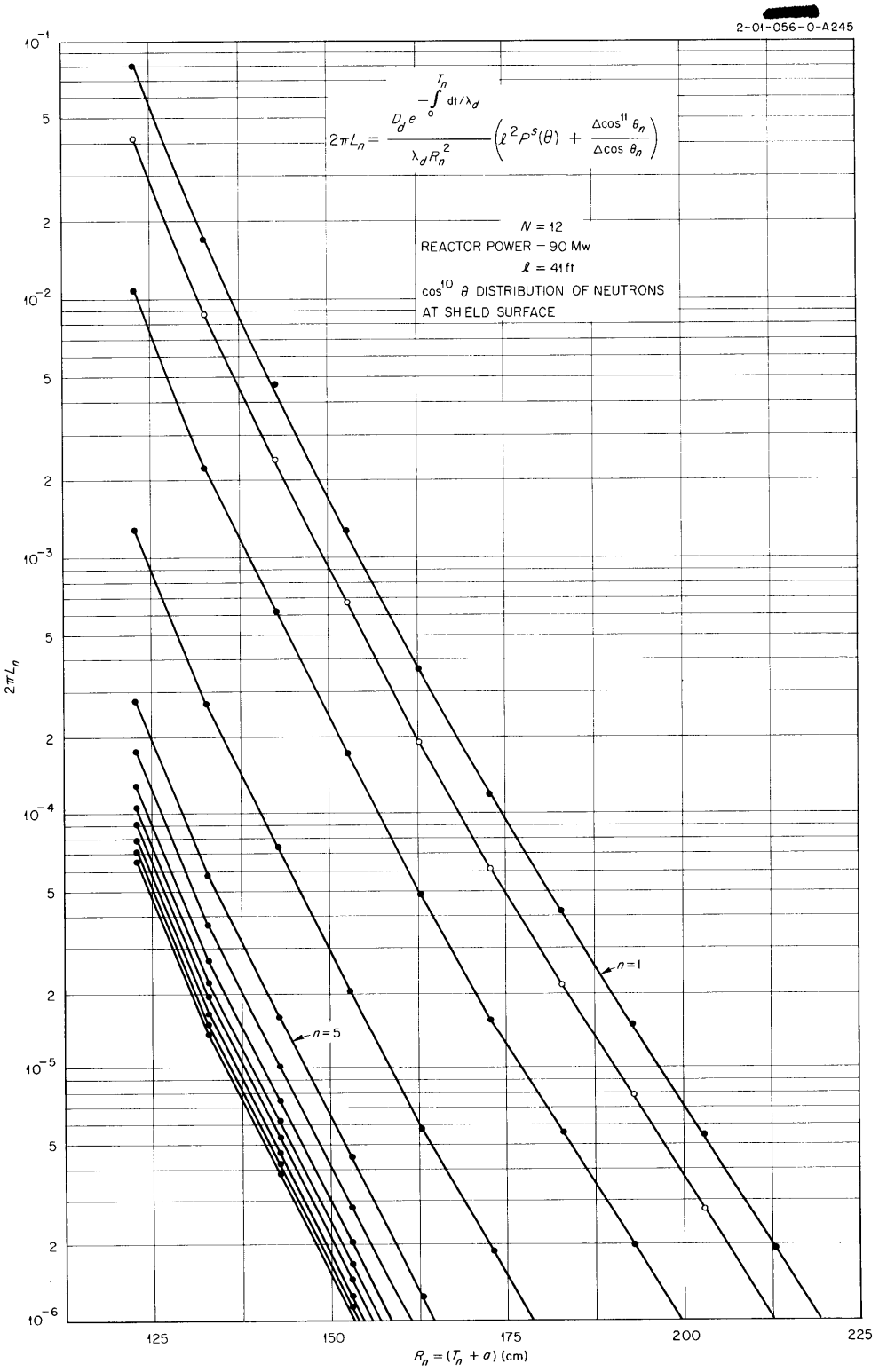

Fig. 14.23. Lagrange Multipliers as a Function of Reactor Shield Radius.

TABLE 14.2. TOTAL DOSE RATES AND NEUTRON SHIELD WEIGHTS FOR VARIOUS LAGRANGE MULTIPLIERS

90-Mw Reactor

$2\pi L$	D_T(Neutrons) at 41 ft (mrem/hr)	Total Water Shield Weight, W_T (lb)
10^{-6}	5.9	39,900
2.5×10^{-6}	13	33,100
5×10^{-6}	24	30,200

TABLE 14.3. RADIUS OF THE UNIT SHIELD FOR EACH CONICAL SHELL

n	θ_n (deg)	R_n (cm)
1	7.5	210
2	22.5	203.5
3	37.5	190.5
4	52.5	170
5	67.5	157
6	82.5	154
7	97.5	151.5
8	112.5	150
9	127.5	148.5
10	142.5	147.5
11	157.5	147
12	172.5	146.5

15. SHIELD WEIGHTS

J. B. Dee
C. A. Goetz H. C. Woodsum
Pratt & Whitney Aircraft
R. M. Davis, The Martin Company
D. R. Otis
Consolidated Vultee Aircraft Corp., San Diego

The calculation of total reactor and divided-shield weights for various 300-Mw circulating-fuel reactors has been completed. The calculation methods and the data used are described, and a table of weights is presented.

DIVIDED-SHIELD WEIGHT DEPENDENCE ON THE DIMENSIONS OF A 300-Mw CIRCULATING-FUEL REACTOR

J. B. Dee J. E. Smolen[1]
C. A. Goetz H. C. Woodsum

The parametric weight study for circulating-fuel reactors has been completed. Total weights of the reactor, reactor shield, and crew-compartment shield were calculated by the shield design method described previously[2] for various power densities, island radii, heat exchanger thicknesses, and reflector thicknesses. These calculations were based on data and analyses of data from Lid Tank Shielding Facility (LTSF) circulating-fuel reflector-moderated reactor (CFRMR) experiments[3,4] and from Tower Shielding Facility (TSF) differential shielding experiments,[5-7] a divided-neutron-shield optimization procedure[7] and the NDA single-scattering penetration probabilities for gamma rays.[8] No attempt has been made here to define completely the terminology, since the definitions were presented in the previous report.[2] Reference to that report will be necessary to an understanding of this report.

Gamma-Ray Shield

Primary Gamma-Ray Dose Rate. – The primary gamma-ray dose rate for a specific reactor and lead-alkylbenzene shield (Table 15.1) was determined from the LTSF CFRMR experimental data. The variation of this dose rate with the thickness of the beryllium reflector, the thickness of the lead gamma shield, and the total shield thickness is plotted in Fig. 15.1. The ordinate represents the dose rate from an infinite plane source.

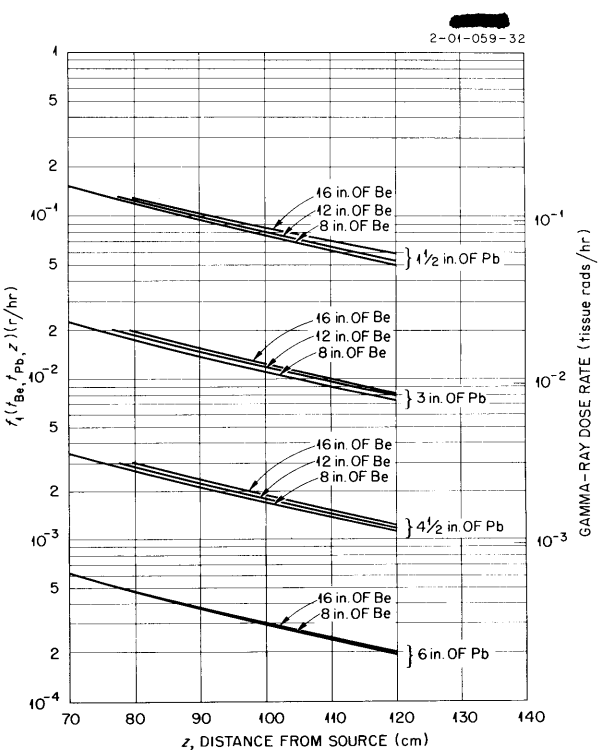

Fig. 15.1. Primary Gamma-Ray Dose Rate in Alkylbenzene from an Infinite Plane Source for a Circulating-Fuel Reactor.

[1] Pratt & Whitney Aircraft; at Lid Tank Shielding Facility.

[2] J. B. Dee *et al.*, *ANP Quar. Prog. Rep. Sept. 10, 1955*, ORNL-1947, p 189.

[3] G. T. Chapman *et al.*, *ANP Quar. Prog. Rep. June 10, 1955*, ORNL-1896, p 194; *ANP Quar. Prog. Rep. Sept. 10, 1955*, ORNL-1947, p 197.

[4] R. W. Peelle *et al.*, Sec. 13, this report.

[5] C. E. Clifford *et al.*, Sec. 14, this report.

[6] C. E. Clifford *et al.*, *ANP Quar. Prog. Rep. June 10, 1955*, ORNL-1896, p 205.

[7] C. E. Clifford *et al.*, *ANP Quar. Prog. Rep. Sept. 10, 1955*, ORNL-1947, p 205.

[8] E. P. Blizard and H. Goldstein (eds.), *Report of the 1953 Summer Shielding Session*, p 167, ORNL-1575 (June 14, 1954).

TABLE 15.1. CFR-SHIELD CONFIGURATION ASSUMED FOR CALCULATIONS OF PRIMARY GAMMA-RAY DOSE RATE

Region	Material	Thickness (in.)
Core shell	Inconel	0.156
Cooling annulus	Sodium	0.187
Reflector	Beryllium	8 12 16
Cooling annulus	Sodium	0.066
Curtain cladding	Inconel X	0.01
Boron curtain	B_4C, $\rho = 2.28$ g/cm^3 Cu, $\rho = 2.69$ g/cm^3	0.20
Curtain cladding	Inconel X	0.01
Cooling annulus	Sodium	0.066
Heat exchanger cladding	Inconel X	0.25
Heat exchanger	25 vol % Ni 75 vol % NaF $\rho = 1.59$ g/cm^3	4.00
Heat exchanger cladding	Inconel X	0.125
Thermal shield	97 wt % Inconel X, 3 wt % B_4C	1.00
Cooling annulus	Sodium	0.035
Pressure shell	Inconel X	1.00
Insulation	Al_2O_3, $\rho = 0.1$ g/cm^3	0.25
Cooling annulus	Alkylbenzene 350	0.375
Gamma shield	Lead	1.00
Cooling annulus	Alkylbenzene 350	0.375
Gamma shield	Lead	Variable*
Neutron shield	Alkylbenzene 350	Variable*

* Thickness to be determined by dose rate desired.

The curves in Fig. 15.1 were used to calculate the primary gamma-ray dose rates for particular spherical reactor shields by means of the expression

$$(1)\quad D_P(d) = \frac{r_c r_s}{d^2} \frac{P_R/4\pi r_c^2}{P_{LT}/\pi a^2} f_1(t_{Be}, t_{Pb}, z)\, f_2(t_{HX_R}),$$

where

$$(2)\quad f_1(t_{Be}, t_{Pb}, z) = H(a,z)\, D_{P\text{-}LT}(a,z)\, c_2 c_3 .$$

In Eq. 1 the function f_2 represents a correction in the attenuation for variations from the heat exchanger composition and thickness given in Table 15.1. The composition of the heat exchanger was taken for this calculation to be 27.3 vol % fuel

(200 lb/[redacted]), 19.1 vol % Inconel (530 lb/ft^3), and 53.6 vol % NaK (46.3 lb/ft^3). Values of f_2 for this composition were calculated for various heat exchanger thicknesses, as follows:

t_{HX_R} (in.)	$f_2(t_{HX_R})$
3.5	1.22
6.5	0.735
8	0.570

Heat Exchanger Gamma-Ray Dose Rate. – The gamma-ray dose rate from the heat exchanger was determined by the expression

$$(3)\quad D_{HX}(d) = v_f \frac{P_R}{V_f} \frac{r_{HX_o} r_s}{d^2} f_3(t_{HX})\, f_4(t_{Pb}, t_s) ,$$

where

t_s = total reactor shield thickness,

$$(4)\quad f_3(t_{HX}) = \lambda(E) \overline{\left\{ 1 - \frac{r_{HX_i}}{r_{HX_o}} e^{-t_{HX}/\lambda(E)} + \frac{\lambda(E)}{r_{HX_o}} \left[e^{-t_{HX}/\lambda(E)} - 1 \right] \right\}} ,$$

$$(5)\quad f_4(t_{Pb}, t_s) = 3.1 \times 10^{10} \int_0^\infty \frac{B(\mu t) E_1(\mu t) N(E)}{2C(E)}\, dE .$$

The function f_3 represents the average product of the heat exchanger self-shielding factor times the relaxation length for fission-product gamma rays emitted from the heat exchanger, and it is plotted in Fig. 15.2. The function f_4 represents the gamma-ray dose rate in alkylbenzene from an infinite plane source of fission products followed by the thermal shield, pressure shell, thermal insulation, and lead. A plot of f_4 is given in Fig. 15.3.

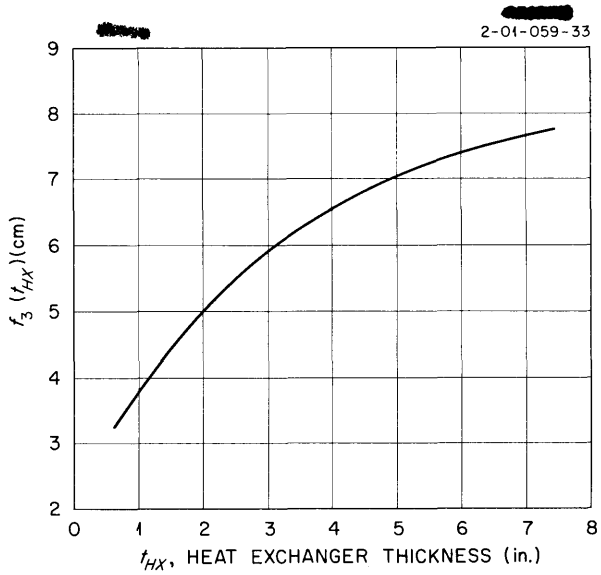

Fig. 15.2. Average Product of the Self-Shielding Factor and the Relaxation Length for Fission-Product Gamma Rays in the Heat Exchanger of a Circulating-Fuel Reactor.

Secondary Gamma-Ray Dose Rate. – The secondary gamma-ray dose rate originating near the lead-alkylbenzene interface was calculated from the expression

$$(6)\quad D_S(d) = f_5(t_{Alky})\, f_6(t_{Be}, t_{Pb})\, f_7(t_{HX}) \frac{r_c r_s}{d^2} e^{-t_l/\lambda_l} H(a, z_{Pb}) \frac{\sigma_R}{\sigma_{LT}} ,$$

where

$$(7)\quad f_5(t_{Alky}) = D_{S\text{-}LT}(12 \text{ in. Be, } 4.5 \text{ in. Pb, } t_{Alky})\, H(a', t_{Alky}) ,$$

$$(8)\quad f_6(t_{Be}, t_{Pb}) = \frac{D_{S\text{-}LT}(t_{Be}, t_{Pb}, t_{Alky})}{D_{S\text{-}LT}(12 \text{ in. Be, } 4.5 \text{ in. Pb, } t_{Alky})} ,$$

$$(9)\quad f_7(t_{HX}) = e^{-(\Sigma_{HX_R} - \Sigma_{HX_{LT}})10.16}\, e^{-\Sigma_{HX_R}(t_{HX} - 10.16)} .$$

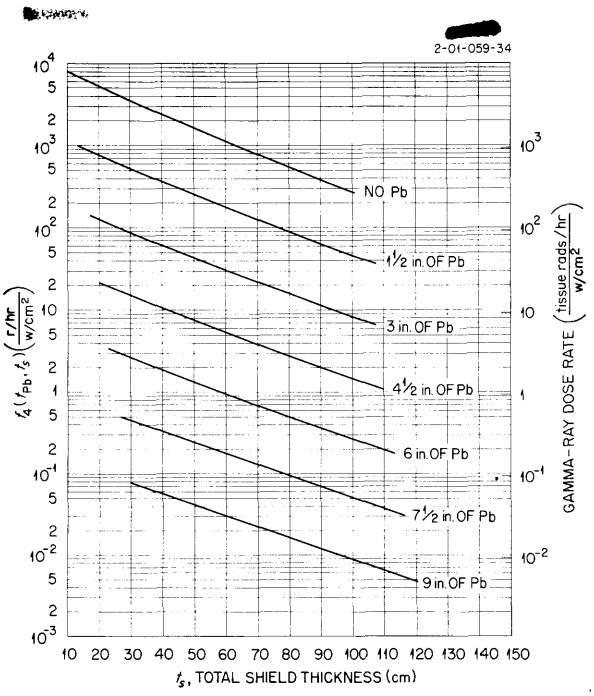

Fig. 15.3. Gamma-Ray Dose Rate in Alkylbenzene from an Infinite Plane Source of Fission Products for a Circulating-Fuel Reactor.

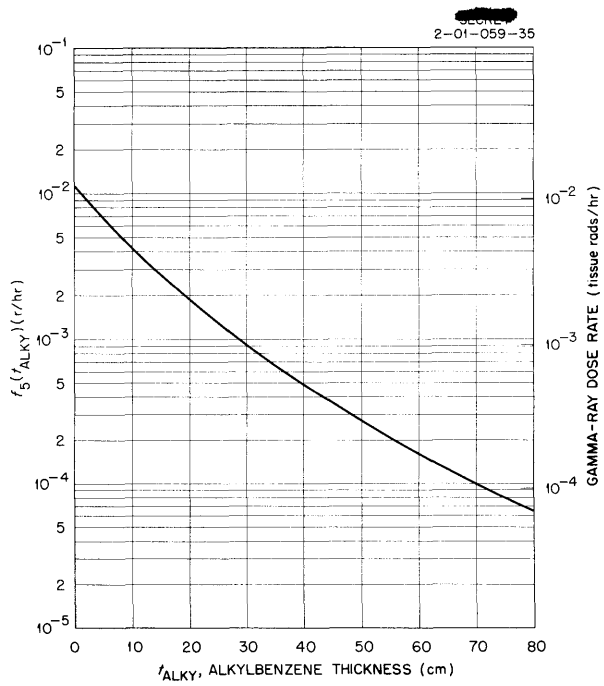

Fig. 15.4. Secondary Gamma-Ray Dose Rate in Alkylbenzene from an Infinite Plane Source for a Circulating-Fuel Reactor.

The function f_5 (Fig. 15.4) is the dose rate in alkylbenzene from an infinite plane source of secondary radiation having the same surface source strength as the LTSF CFRMR configuration containing 12 in. of beryllium and 4.5 in. of lead. For other thicknesses of beryllium and lead, the curve was found to have the same shape but to differ by a constant multiplier, f_6, which is listed in Table 15.2. The function $f_7(t_{HX})$ is a correction for the heat exchanger thickness.

Total Gamma-Ray Dose Rate. – The total gamma-ray dose rate in the crew compartment, $D_{\Gamma_{cc}}$, was taken as the sum of the dose rates from direct and scattered gamma rays entering the rear and sides of the crew compartment:

$$(10) \quad D_{\Gamma_{cc}} = D_{PDR} + D_{PSS} + D_{SDR} + D_{SSS} ,$$

where

D_{PDR} = dose rate from direct primary plus direct heat exchanger gamma rays entering the rear,

TABLE 15.2. CORRECTION FACTOR f_6 APPLIED TO SECONDARY GAMMA-RAY DOSE RATE FOR VARIATIONS IN LEAD AND BERYLLIUM THICKNESSES

Lead Thickness (in.)	$f_6(t_{Be}, t_{Pb})$		
	8 in. of Beryllium	12 in. of Beryllium	16 in. of Beryllium
1.5	4.7	1.6	0.32
3.0	4.3	1.3	0.26
4.5	3.9	1.0	0.21
6.0	3.5	0.76	0.17

D_{PSS} = dose rate from air-scattered primary plus air-scattered heat exchanger gamma rays entering the sides,

D_{SDR} = dose rate from direct secondary gamma rays entering the rear,

D_{SSS} = dose rate from air-scattered secondary gamma rays entering the sides.

This [redacted]ation does not include the dose rate from air-scattered gamma rays entering the rear, which were found to be unimportant, nor does it include a dose rate from the radioactive NaK circulated to the engines, which was also found to have a negligible effect. The radiation scattered into the front of the crew compartment was ignored. It was assumed that a front shield having the same composition as the side shield would be more than adequate.

The direct dose rate D_{PDR} from gamma rays entering the crew compartment rear wall was assumed to be attenuated by lead and plastic with the same relaxation length that was effective at the reactor shield location. From the LTSF tests, the gamma-ray relaxation length for lead, λ_{Pb}, is 2.1 cm. The gamma-ray relaxation length for water, λ_{H_2O}, is 43 cm. This corresponds to an average λ_{pl} value of 30 cm for polyethylene plastic, when the decreased electron density is taken into consideration. As described in the previous report,[2] a basic gamma-ray shield was wrapped around the reactor to maintain a minimum radiation level outside the reactor consistent with radiation-damage requirements, $D_o(d)$. The direct dose rate from primary and heat exchanger gamma rays entering the crew compartment rear, expressed in terms of $D_o(d)$, then is

$$(11)\quad D_{PDR} = D_o(d)\, e^{-t_{pl}/\lambda_{pl}}\, e^{-t_R/\lambda_{Pb}}\, e^{-t_r/\lambda_{Pb}} ,$$

where

$D_o(d)$ = $D_{HX}(d) + D_P(d)$ for the basic shield,

t_{pl} = plastic thickness on the rear of the crew compartment,

t_R = thickness of lead in the shadow shield,

t_r = thickness of lead on the rear of the crew compartment.

The dose rate from primary and heat exchanger gamma rays scattered into the sides of the crew compartment, D_{PSS}, was calculated as the sum of several components. As mentioned previously,[2] an approximation for the effect of the angular distribution of the gamma rays escaping from the reactor shield surface was made by assuming a "disadvantage angle" α (Fig. 15.5) when calculating the scattered radiation penetrating the crew compartment. This assumption results in a constant-thickness portion of the shadow shield that subtends a half-angle α with respect to the reactor-to-crew-compartment axis, followed by a tapered section that decreases linearly in thickness, with the angle θ, until it reaches zero. The contribution from the portion of the shadow shield with a uniform thickness, which has an angular half-width α, was expressed as

$$(12)\quad D_{PSS_1} = e^{-t_R/\lambda_R}\, D_o(d)\, 4\pi d^2\, \frac{1500}{d}\, C\, f(E_0,0,d) \int_0^{\alpha} d\theta ,$$

where

$1500/d$ = inverse distance correction to apply scattering probability to separation distance d(cm),

C = number of Mev/cm^2-sec equal to 1 r/hr (6.75×10^5 at $E_0 = 6mc^2$),

$f(E_0,\psi,d)$ = single air-scattering penetration probability for a separation distance of 50 ft for emission direction ψ with respect to the reactor-to-crew-compartment axis, and for photon energy E_0 (here taken to be $6mc^2$ or 3 Mev).

The tapered portion of the shadow shield was chosen to decrease in thickness, $t_R'(\theta)$, to permit the product of the dose-rate emission times the scattering-penetration probability to be constant:

$$(13)\quad t_R'(\theta) = t_R - \frac{(\theta - \alpha)}{\lambda_\psi}\lambda_{Pb} ,$$

where

α = 0.262 radian,[9]

λ_ψ = relaxation angle for the scattering-penetration probability

= 0.218 radian, as defined by the expression

$$(14)\quad f(E_0,\psi,d) = f(E_0,0,d)\, e^{-\psi/\lambda_\psi} .$$

The edge of the shadow shield is found at θ_0 as given by

$$(15)\quad \theta_0 = t_R \frac{\lambda_\psi}{\lambda_{Pb}} + \alpha .$$

[9] Recent calculations indicate that $\alpha = 0.09$ radian is a more realistic value.

[redacted]
2-01-059-37

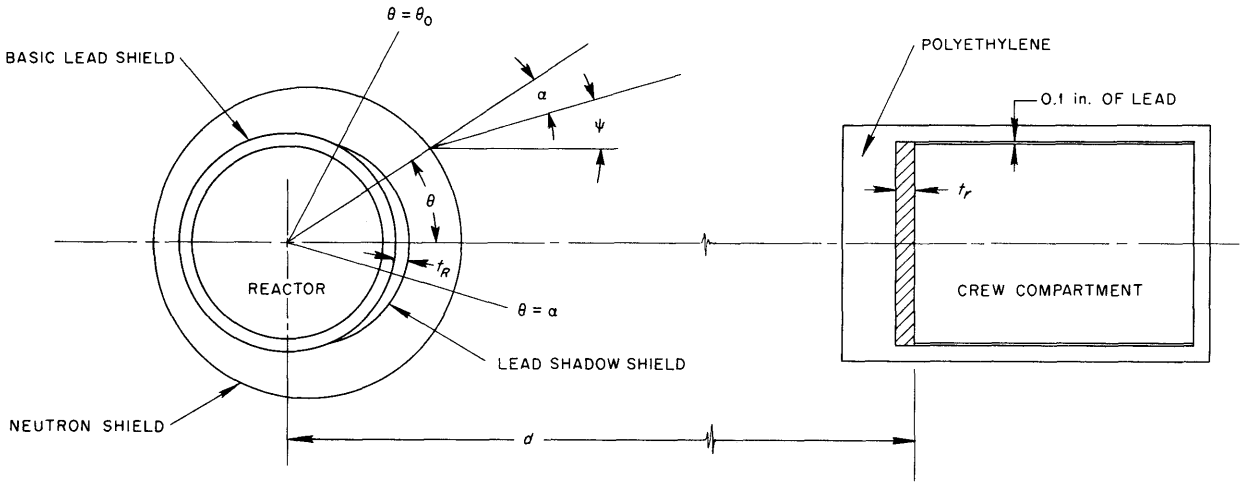

Fig. 15.5. Geometry for Divided-Shield Gamma-Ray Calculations.

The dose rate from primary gamma rays emitted from the tapered portion of the shadow shield is thus

$$D_{PSS_2} = e^{-t_R/\lambda_R} D_o(d)\, 4\pi d^2 \frac{1500}{d} C \int_\alpha^{\theta_0} e^{(t_R - t_R')/\lambda_{Pb}} f(E_0, \theta-\alpha, d)\, d\theta \ . \tag{16}$$

From the remainder of the gamma shield the contribution is

$$D_{PSS_3} = e^{-t_R/\lambda_R} D_o(d)\, 4\pi d^2 \frac{1500}{d} C \int_0^{\pi} e^{t_R/\lambda_{Pb}} f(E_0, \theta-\alpha, d)\, d\theta \ . \tag{17}$$

Adding the separate contributions and simplifying, the total dose rate from air-scattered primary and heat exchanger gamma rays penetrating the crew-compartment sides is

$$D_{PSS} = e^{-t_R/\lambda_R} D_o(d)\, 4\pi d^2 \frac{1500}{d} C(\theta_0 + \alpha) f(E_0, 0, d) \ . \tag{18}$$

The dose rate from direct secondary gamma rays entering the rear of the crew compartment was calculated for the basic shield. These gamma rays are attenuated by the crew-compartment rear and also by the alkylbenzene annulus separating the shadow shield from the basic shield, and the dose rate is thus

$$D_{SDR} = D_S(d, \text{basic shield})\, e^{-t_a/\lambda_a} e^{-t_{pl}/\lambda_{pl}} e^{-t_r/\lambda_{Pb}} , \tag{19}$$

where

t_a = annulus thickness,

λ_a = relaxation length of the alkylbenzene in the annulus for secondary gamma rays (5.33 cm as reported previously for the gamma-ray-shield cooling layers).

The dose rate from scattered secondary gamma rays penetrating the sides of the crew compartment was estimated by assuming an isotropic source whose strength is determined by the source intensity in the forward part of the reactor shield:

$$D_{SSS} = D_S(d, \text{basic shield})\, e^{-t_l/\lambda_l}\, 4\pi d^2 \frac{1500}{d} C \int_0^{\pi} f(E_0, \psi, d)\, d\psi \ . \tag{20}$$

Neutron Shield

The dose rate due to neutrons emitted from the reactor shield was calculated from the following expression:

$$D_n(d) = f_8(t_{Be}, z) \frac{r_c r_s}{d^2} \frac{\sigma_R}{\sigma_{LT}} e^{-(\Sigma_{HX_R} - \Sigma_{HX_{LT}})^{10.16}} e^{-(\Sigma_{HX_R} - \Sigma_{Alky})(t_{HX} - 10.16)} . \tag{21}$$

The function f_8 (Fig. 15.6) represents the LTSF fast-neutron dose rate which has been corrected for small differences in materials for alkylbenzene and has been transformed to infinite plane geometry:

$$f_8(t_{Be}, z) = D_n(t_{Be}, z)\, H(z)\, e^{-\delta\Sigma t_R} e^{(\Sigma_{H_2O} - \Sigma_{Alky}) t_{Alky}} . \tag{22}$$

[10] E. P. Blizard and H. Goldstein (eds.), *Report of the 1953 Summer Shielding Session*, p 345, ORNL-1575 (June 14, 1954).

Total Shield Weights

Total reactor, reactor-shield, and crew-compartment-shield weights were calculated for various 300-Mw circulating-fuel reactors and are listed in Table 15.3. In calculating these total weights, allowances for patches over fuel and NaK ducts were made according to early published estimates.[10] A structural weight of 2500 lb was calculated for an 80,000-lb reactor and shield. The variation with the integral shield weight was taken to be $[42.4 + (W/10{,}400)]^2$, where W is the weight of the reactor shield and its contents.

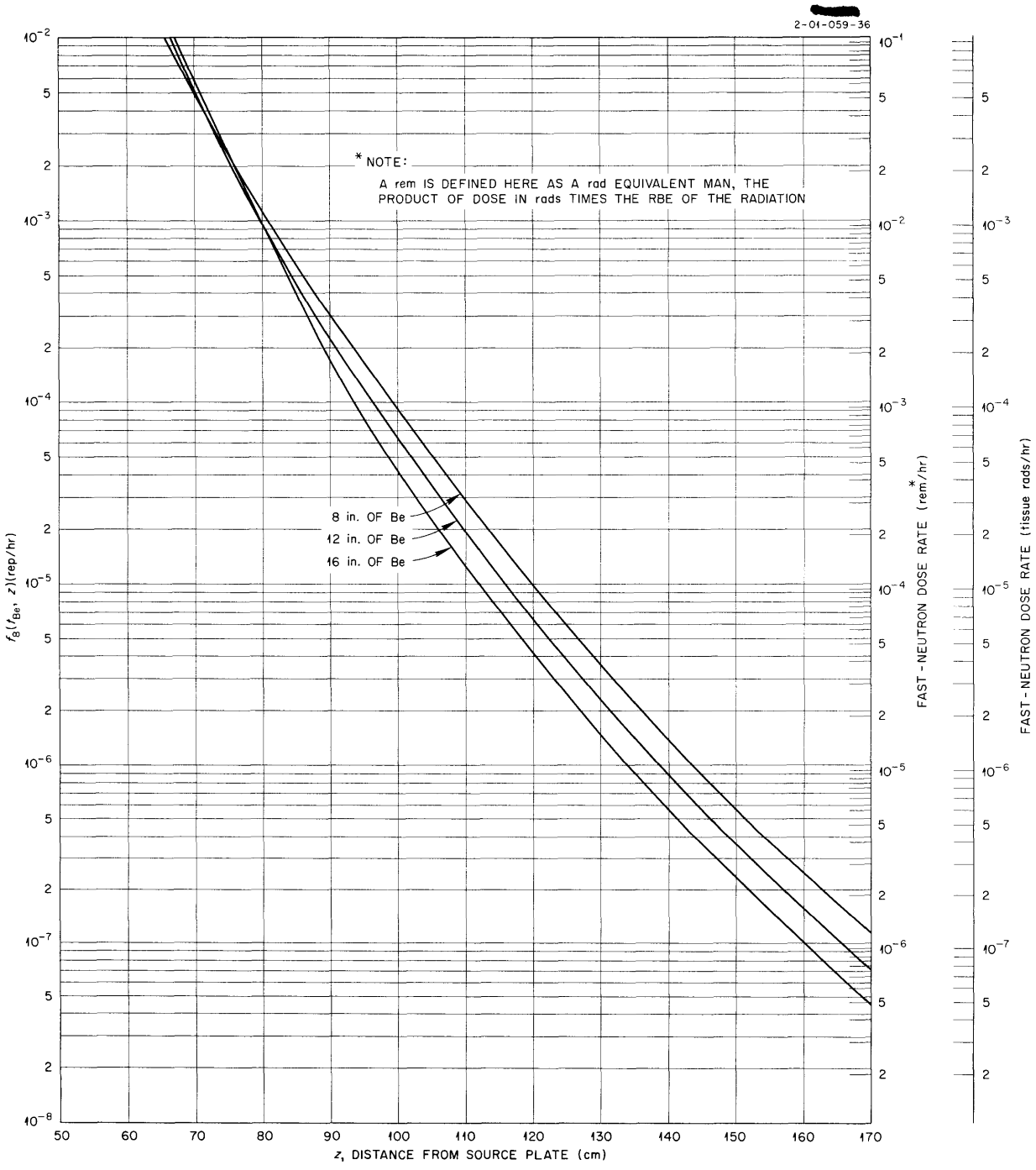

Fig. 15.6. Fast-Neutron Dose Rate in Alkylbenzene from an Infinite Plane Source for a Circulating-Fuel Reactor.

TABLE 15.3. REACTOR AND SHIELD WEIGHTS AS A FUNCTION OF THE DIMENSIONS OF A 300-Mw CIRCULATING-FUEL REACTOR

Dose rate inside crew compartment: 1 rem/hr

Power Density (kw/cm^3)	Island Radius (in.)	Heat Exchanger Thickness (in.)	Total Weight ($lb \times 10^{-3}$) of Reactor, Reactor Shield, and Crew Compartment Shield			
			8-in. Reflector Thickness	10-in. Reflector Thickness	12-in. Reflector Thickness	16-in. Reflector Thickness
1.375	0	3.5	67.2	69.8	73.0	80.5
		6.5	72.8	75.7	79.3	88.0
		8.0	75.3	78.5	82.7	92.3
	4	3.5	68.5	71.4	74.3	82.3
		6.5	73.9	77.3	80.5	89.9
		8.0	76.8	80.5	84.3	94.3
	8	3.5	71.4	74.6	78.2	87.2
		6.5	77.3	80.9	85.0	94.7
		8.0	80.4	84.1	88.7	99.1
2.750	0	3.5	60.3	62.9	65.8	72.9
		6.5	65.0	67.9	71.6	79.5
		8.0	67.6	70.7	74.8	83.5
	4	3.5	61.4	64.2	67.2	74.6
		6.5	66.2	69.4	73.0	81.5
		8.0	68.9	72.4	76.1	85.4
	8	3.5	65.6	68.7	71.9	80.4
		6.5	70.7	74.3	78.1	87.7
		8.0	73.5	77.4	81.4	91.3
4.125	0	3.5	57.9	60.5	63.3	70.1
		6.5	62.4	65.4	68.6	76.7
		8.0	65.0	68.1	71.6	80.0
	4	3.5	59.0	61.7	64.8	71.8
		6.5	63.8	66.8	70.2	78.4
		8.0	66.2	69.6	73.3	82.1
	8	3.5	63.3	66.4	69.7	77.7
		6.5	68.4	71.9	75.6	84.9
		8.0	71.1	74.8	78.8	88.9
5.500	0	3.5	56.0	58.4	61.4	68.1
		6.5	60.4	63.3	66.5	74.3
		8.0	62.7	66.0	69.3	77.7
	4	3.5	57.3	60.0	62.9	69.9
		6.5	61.8	64.9	68.2	76.3
		8.0	64.3	67.6	71.2	79.8
	8	3.5	62.0	65.0	68.3	76.3
		6.5	66.9	70.3	74.0	83.2
		8.0	69.5	73.2	77.2	87.2

[redacted]

[redacted]